Computational Materials Genome Initiative by High-Throughput Approaches

by

Junkai Xue

Department of Mechanical Engineering and Materials Science
Duke University

Date: _____

Approved:

_____
Stefano Curtarolo, Supervisor

_____
Omar M. Knio

_____
Walter N. Simmons

_____
Nico Hotz

Dissertation submitted in partial fulfillment of the requirements for the degree of Doctor of Philosophy in the Department of Mechanical Engineering and Materials Science
in the Graduate School of Duke University
2013

Abstract

Computational Materials Genome Initiative by High-Throughput Approaches

by

Junkai Xue

Department of Mechanical Engineering and Materials Science
Duke University

Date: _____

Approved:

_____
Stefano Curtarolo, Supervisor

_____
Omar M. Knio

_____
Walter N. Simmons

_____
Nico Hotz

An abstract of a dissertation submitted in partial fulfillment of the requirements for the degree of Doctor of Philosophy in the Department of Mechanical Engineering and Materials Science
in the Graduate School of Duke University
2013

Abstract

Recently, in materials innovations, computational methods are used more frequently than in past decades. In this thesis, the materials genome initiative, an advanced new framework, will be introduced. With this blueprint, our efficient high-throughput software, AFLOW, has been implemented with several compatible functions for materials properties investigations, such as prototype searching, phase diagram studying and magnetic properties discovering. With this effective tool, we apply *ab initio* calculations to discover new generation of specific materials properties.

An efficient algorithm for prototypes comparision has been designed and implemented into our high-throughput framework AFLOW. In addition, prototypes classification was utilized to differentiate the our materials database. This classification will accelerate the materials properties searching speed. With respect to structure prototypes, low temperature phase diagrams were used for binary and ternary alloy systems stability investigation. The alogrithms have been integrated into AFLOW. With this tool, we systematically explored the binary Ru systems and Tc systems and predicted new stable compounds.

Contents

List of Tables

List of Figures

Acknowledgements

I would like to thank my advisor, Dr. Stefano Curtarolo, for the guidance and support he showed me throughout my thesis writing. Besides I also would like to thank Shidong Wang, Kesong Yang, Chenging Chia, Richard Taylor, Kevin Rasch and Camilo Calderon for their help. Finally, the understanding and patience shown by my family is greatly appreciated.

1

Introduction

Recently, the advancement of science and technology has been hindered in many areas because of the lack of appropriate materials. Thus, an integral part of the ongoing effort in science is material innovation. This effort has led to a new concept, the materials genome initiative, that was inspired by the use of DNA as a blueprint for biological organisms. This materials genome initiative provides a path for developing a broad framework for material discovery. To implement this initiative, some fundamental groundwork must be laid, which includes the development of computational and experimental techniques and methods to manipulate large amounts of data. As part of this effort, our work involved developing computational methods and constructing large databases.

1.1 High-throughput software - AFLOW

We implemented several efficient algorithms in our high-throughput (HT) framework AFLOW, which is a next-generation software designed to discover material properties and is based on *ab initio* calculations. We propose to calculate materials properties and optimize data by using the Vienna Ab Initio Simulation Package (VASP) [Kresse

and Hafner (1993)], which is based on *ab initio* density functional theory (DFT). VASP uses the projector-augmented-wave (PAW) method [Gajdoš et al. (2006)] or pseudopotentials and a plane-wave basis set [Kresse and Hafner (1993)]. By using the local density approximation, VASP relaxes crystal structures by accurately estimating the ground states. By integrating VASP into the AFLOW framework, DFT can be applied to a single structure or to sets of structures by using stored data or data obtained from incomplete calculations.

AFLOW automates the calculation of large-scale structures; it requires less human intervention and provides a suite of physical observables over a specified class. The software also allows the user to set up standardized calculations for special cases. To optimize the accuracy of the large quantity of data produced by the HT approach (and therefore the credibility of the results), the entire process must be executed in a consistent and robust manner. It is important for AFLOW to strictly follow this rule, because the target is to simultaneously optimize multiple material properties for diverse applications. In particular, electronic structure and thermodynamics properties are important for the development of superconductors and catalysts of materials [Kolmogorov et al. (2008); Wolverton et al. (2008)]. By simply launching AFLOW as a Unix daemon through the queue query of a computer cluster severer, AFLOW can generate data, run them through the algorithm, and obtain convergence to obtain a large set of results in a single day and with minimum manual intervention.

The principal function of this tool is to differentiate between stable and metastable structures by optimally relaxing the ground-state energy. It also offers numerous qualified functions, including electronic-band-structure visualization, phonon spectra detection, reconstruction of phase diagrams, optimization of vibrational free energy, expansion of the atomic environment [Daams et al. (1992)], and classification of the crystal-structure prototype. For example, AFLOW uses three distinct methods to simulate phonon dispersion curves, including the PAW linear response method, the

frozen-phonon method (which is implemented by FROZSL [Boyer et al. (1995)]), and the direct force-constant method [Maradudin et al. (1971)]. Each of these approaches is appropriate for different research purposes. By using these powerful methods, we investigate materials properties in different situations. Note that AFLOW is still under construction; hence, new applications will be periodically integrated into the source code.

Recently, the most difficult challenge has been that the automatically generated HT database terminates because of the failure of a single calculation. The likely cause of this phenomenon is limited hardware resources. To circumvent the problem, we preprocess the data and analyze the strategy. For instance, to avoid conflict between different tasks and group jobs when they run on the same computer node, we must roughly estimate the memory requirements. In addition, interruptions caused by runtime errors of the *ab initio* calculation itself also terminate the process. The *ab initio* errors involve incorrect geometries, inconsistent atom locations, inconsistent reciprocal and k lattice meshes, and invalid input, to name a few. AFLOW automatically detects most of these errors and attempts to correct the input and rerun the calculation. This process is implemented by tracking the error message, rebuilding the appropriate input, and restarting the *ab initio* calculation.

The AFLOW database contains over 400 experimental crystal-structure prototypes extracted from the Navy Crystal Lattice Database [Mehl (2012)], the Inorganic Crystal Structures Database (ICSD) [Mighell and Karen (1993); Karen and Hellenbrandt (2002); Brown et al. (2005); Belsky et al. (2002)], and the Pauling File [Villars et al. (2004)]. The majority of these prototypes are quickly generated by the online AFLOW tool (1.1) or by the Linux command-line version of AFLOW. Sometimes the relaxed crystal structures (basis, shape, side-cell volume) generated by AFLOW appear to be ground states that do not exist in the experimental prototype lists [Curtarolo et al. (2005)]. In such cases, the structures are added to the structure

database.

FIGURE 1.1: Screenshot of AFLOW online tool.

The AFLOW database contains a few million fcc- and bcc-derived superstructures, which contain over 20 atoms per lattice cell. Similar to hcp-derived superstructures, these structures are formulated by the algorithm from Refs. [Hart and Forcade

(2008)] and [Hart and Forcade (2009)]. In fact, only several hundred of these crystal structures are used to construct alloy systems, but their use is advantageous for expanding clusters [Sanchez et al. (1984); Gus L. W. Hart and Zunger (2005); Lerch et al. (2009)].

1.2 Materials database - AFLOWLIB.ORG

In addition to developing AFLOW, we also developed a materials database, which is a difficult task because of the large number of crystal-structure frames and element combinations involved. To obtain geometrical information and other properties of materials, researchers usually depend on empirical data from commonly used experimental databases such as ICSD, the Pauling File Inorganic Materials Database, Pearson's Crystal Data [P. Villars (1991)], and CRYSTMET [White et al. (2002)]. Although these databases contain large quantities of data, their datasets are not complete. Many reasons may explain this observation; the main one being that the material synthesis strategy calls for long equilibration times and high temperature and pressure. Thus, to discover modern materials, computational databases are required.

The computational materials database generated by AFLOW [Curtarolo et al. (2012a)] is called **aflowlib.org** and contains the following repositories:

1. alloy systems including energies, ground states, unstable structures, and phase diagrams (currently, most of the phase diagrams are binary);

2. electronic information on inorganic materials such as electronic band structure, effective mass, etc.;

3. magnetic properties including spin polarizations, magnetic moments, and other related parameters.

The construction of this online-based database is ongoing and diverse data continue to be added on a regular basis.

1.2.1 Alloy systems

For alloy systems, the HT framework AFLOW generates input files and runs the *ab initio* calculations. Almost 650 binary alloy systems containing over 150,000 distinct compounds, including metals, alkali metals, and transition metals, have been generated. The system also generates crystal structure space groups, the *Strukturbericht* designation or crystal structure prototypes, and ground-state energies. This information is available by accessing our online database **aflowlib.org** (1.2), where the following options are displayed:

1. **all**: This option allows the user to generate complete data for a given binary system. The data for original structures and relaxed structures are produced by AFLOW and the output is presented as a webpage (1.3). Fig. 1.4 demonstrates the list of relaxed structures for the AsGe system with an As concentration of 0.5. In the second line, we list the ground state of the system with the prototype of the structure. In addition, the label "Emin-GND" will addict to that structure. The list also enables differentiating original structures from relaxed structures. For instance, at line 4, the structure begins as prototype Pd_2Ti (space group 74) but changes into prototype $C11_b$ (space group 139).

2. **commonly used lattices**: Several widely used lattice types exist, such as fcc, bcc, and hcp. The software can generate the systems with these listed lattices, which is very powerful for cluster expansions [Nakatsuji (1978)].

3. **binary low-temperature phase diagrams**: Zero-temperature phase diagrams are constructed from the formation enthalpies of a large number of crystal structures. These formation enthalpies in turn are automatically computed

by AFLOW from the results of the *ab initio* calculations. Based on these enthalpies, AFLOW applies an efficient algorithm to establish the binary convex hull and produces the low-temperature phase diagrams. The details of the low-temperature phase diagrams are introduced in Chapter 3.

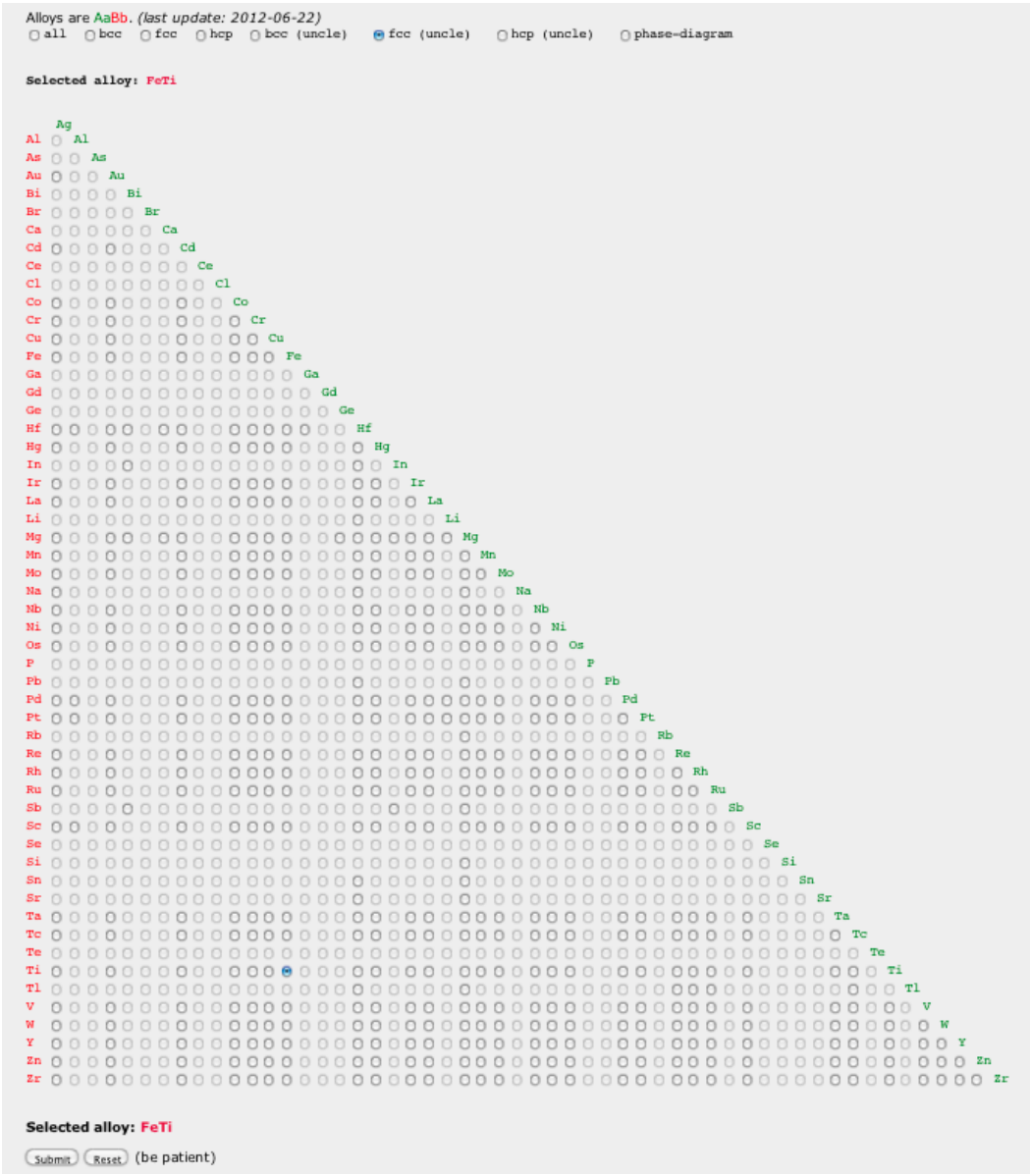

FIGURE 1.2: Interface of online binary alloy database.

```
[FeTi/137] # ************************************************************
[FeTi/137] # ------------------------------------------------------------
[FeTi/137] FeTi/137
[FeTi/137] # Structure PRE ------------------------------------------
[FeTi/137] Fe_pvTi_sv.137
[FeTi/137] -90.351500
[FeTi/137]   -0.50000000000000   0.86602540000000  -1.63299320000000
[FeTi/137]    0.50000000000000   0.86602540000000  -1.63299320000000
[FeTi/137]    0.00000000000000  -3.46410160000000   1.63299320000000
[FeTi/137] 2 4
[FeTi/137] Direct(6) [A2B4]
[FeTi/137]    0.11111111111111   0.11111111111111   0.72222222222222  Fe_pv+5
[FeTi/137]    0.66666666666667   0.66666666666667   0.33333333333333  Fe_pv+5
[FeTi/137]    0.00000000000000   0.00000000000000   0.00000000000000  Ti_sv+5
[FeTi/137]    0.33333333333333   0.33333333333333   0.66666666666667  Ti_sv+5
[FeTi/137]    0.44444444444444   0.44444444444444   0.38888888888889  Ti_sv+5
[FeTi/137]    0.77777777777778   0.77777777777778   0.05555555555556  Ti_sv+5
[FeTi/137] # Structure POST -----------------------------------------
[FeTi/137] Fe_pvTi_sv.137
[FeTi/137] 2.771829
[FeTi/137]   -0.53785981042122   0.83977299906172  -1.59382469624609
[FeTi/137]    0.53785981042122   0.83977299906172  -1.59382469624609
[FeTi/137]    0.00000000000000  -3.19087555264994   1.65609425024619
[FeTi/137] 2 4
[FeTi/137] Direct(6) [A2B4]
[FeTi/137]    0.13875323244943   0.13875323244943   0.77807755392685
[FeTi/137]    0.63902454532835   0.63902454532835   0.27747800162871
[FeTi/137]    0.96615904328719   0.96615904328719   0.95241018298471
[FeTi/137]    0.31127059483969   0.31127059483969   0.60268204064326
[FeTi/137]    0.46650718293809   0.46650718293809   0.45287351491229
[FeTi/137]    0.81161873449059   0.81161873449059   0.10314537257085
[FeTi/137] # ------------------------------------------------------------
[FeTi/137]  -50.07520000000000  # H [eV] (VASP)
[FeTi/137]  -8.34587000000000   # H/at [eV] (VASP)
[FeTi/137]  -0.23550300000000   # Hf/at [eV] (VASP)
[FeTi/137]  -0.00007305000000   # Mom/at
[FeTi/137]  14.10770000000000   # Volume/at
[FeTi/137]   0.33333333333333   # Ca
[FeTi/137]   0.66666666666667   # Cb
[FeTi/137]         C2/m #12     # space group PRE
[FeTi/137]      I4/mmm #139     # space group POST  XX
[FeTi/137] # ************************************************************
```

FIGURE 1.3: Structure data containing label, lattice vectors, and element information.

The binary alloy systems are used for theoretical investigations of structure stabilities. By comparing the results of these theoretical investigations with experimental data, we can determine the accuracy of our predictions of new compounds. For example, we selected Mg binary systems by mixing Mg with 34 other elements [Taylor et al. (2011)]. Over one third of these 34 systems are consistent with experimental results and have even led to predictions of new compounds. Furthermore, seven systems should phase separate according to experimental results [Baker et al. (1986)]. However, our results indicate that these systems can form stable phases. Thus, the

```
1-CONCENTRATION=0.6666667
 *str=    188 Ef=-0.2571 dEf=0.0000 sg=[    Cmcm #63|    Cmcm #63]   C49 ZrSi_{2} (0.0) Emin
 *str=    150 Ef=-0.2552 dEf=0.0019 sg=[    Cmcm #63|    Cmcm #63]   ZrSi_{2} OC12 (0.0)
  str= 657.BA Ef=-0.2382 dEf=0.0190 sg=[    Immm #71| I4/mmm #139]XX Pd_{2}Ti oI6 (0.0)
  str=    232 Ef=-0.2360 dEf=0.0211 sg=[ I4/mmm #139| I4/mmm #139]   C11_b MoSi_{2} BCC_{AB2}^{[001]} (0.0)
  str=    287 Ef=-0.2359 dEf=0.0213 sg=[ I4/mmm #139| I4/mmm #139]   CuZr_{2} (0.0)
  str=    137 Ef=-0.2355 dEf=0.0216 sg=[    C2/m #12| I4/mmm #139]XX 137 (0.0)
  str=      5 Ef=-0.2354 dEf=0.0217 sg=[ I4/mmm #139| I4/mmm #139]   \beta1 FCC_{AB2}^{[100]} (0.0)
  str=     66 Ef=-0.2354 dEf=0.0217 sg=[ I4/mmm #139| I4/mmm #139]   C11_b MoSi_{2} BCC_{AB2}^{[001]} (0.0)
  str=      7 Ef=-0.2345 dEf=0.0227 sg=[    Immm #71| I4/mmm #139]XX MoPt2 (0.0)
  str=    261 Ef=-0.2221 dEf=0.0350 sg=[  Fd-3m #227|  Fd-3m #227]   NiTi_{2} (0.0)
  str=    147 Ef=-0.2118 dEf=0.0453 sg=[    Cmcm #63| I4/mmm #139]XX 147 (0.0)
  str=    211 Ef=-0.2054 dEf=0.0517 sg=[    Pnma #62|    Pnma #62]   C37 Co_{2}Si (0.0)
  str=    234 Ef=-0.1825 dEf=0.0747 sg=[ I4/mcm #140| I4/mcm #140]   C16 Al_{2}Cu (0.0)
  str=    231 Ef=-0.1822 dEf=0.0749 sg=[ I4/mcm #140| I4/mcm #140]   C16 Al_{2}Cu (0.0)
  str=    270 Ef=-0.1739 dEf=0.0833 sg=[ P6/mmm #191|  P-3m1 #164]XX C6 CdI_{2} (0.0)
  str=     62 Ef=-0.1716 dEf=0.0855 sg=[  P-3m1 #164|  P-3m1 #164]   BCC_{AB2}^{[211]} (0.0)
  str=    134 Ef=-0.1256 dEf=0.1315 sg=[    C2/m #12|    C2/m #12]   134 (0.2)
  str=    208 Ef=-0.1102 dEf=0.1469 sg=[P63/mmc #194|P63/mmc #194]   C22 Fe_{2}P (0.0)
  str=    135 Ef=-0.0973 dEf=0.1598 sg=[    C2/m #12|    C2/m #12]   135 (0.0)
  str=    133 Ef=-0.0509 dEf=0.2062 sg=[       Cm #8|       Cm #8]   133 (0.0)
  str=    276 Ef=-0.0227 dEf=0.2345 sg=[P63/mmc #194|P63/mmc #194]   Ni_{2}Si (0.0)
  str=    274 Ef=-0.0214 dEf=0.2357 sg=[P63/mmc #194|P63/mmc #194]   B8_{2} (0.0)
  str=    382 Ef=-0.0172 dEf=0.2400 sg=[I41/amd #141|I41/amd #141]   Ga_{2}Hf (0.1)
  str=    249 Ef=-0.0093 dEf=0.2478 sg=[I41/amd #141|I41/amd #141]   C_c ThSi_{2} (0.0)
  str=      9 Ef=+0.0349 dEf=0.2920 sg=[  P-3m1 #164|  P-3m1 #164]   \alpha1 FCC_{AB2}^{[111]} (0.0)
  str=    284 Ef=+0.0663 dEf=0.3234 sg=[I41/amd #141|I41/amd #141]   GdSi-2(1.) (0.0)
  str=    257 Ef=+0.0701 dEf=0.3272 sg=[    Pnnm #58|    Pnnm #58]   C18 marcasite FeS_{2} (0.0)
  str=    267 Ef=+0.0701 dEf=0.3272 sg=[    Pnnm #58|    Pnnm #58]   C18 marcasite FeS_{2} (0.0)
  str=    281 Ef=+0.0755 dEf=0.3326 sg=[   Pa-3 #205|   Pa-3 #205]   C2 pyrite FeS_{2}  (0.0)
  str=    390 Ef=+0.0845 dEf=0.3416 sg=[ P4/mmm #123| P4/mmm #123]   Hg_{2}Pt (0.0)
  str=    216 Ef=+0.1285 dEf=0.3856 sg=[ P6/mmm #191| P6/mmm #191]   C32 AlB_{2} (0.3)
  str=    246 Ef=+0.1286 dEf=0.3857 sg=[ P6/mmm #191| P6/mmm #191]   hP6 CaIn_{2} (0.3)
  str=    190 Ef=+0.3009 dEf=0.5580 sg=[  P-3m1 #164|  P-3m1 #164]   \Omega Z=14 (0.0)
  str=    315 Ef=+0.4104 dEf=0.6675 sg=[P63/mmc #194|P63/mmc #194]   C36 MgNi_{2} (0.3)
  str=    183 Ef=+0.4179 dEf=0.6750 sg=[  Fd-3m #227|  Fd-3m #227]   C15 Cu_{2}Mg (0.3)
  str=    178 Ef=+0.5114 dEf=0.7685 sg=[P63/mmc #194|P63/mmc #194]   C14 MgZn_{2} (0.0)
```

FIGURE 1.4: Each line in the list gives an original structure and the corresponding relaxed structure.

predicted structures are worthy of use in advanced materials.

In addition to the Mg systems, we also investigated systems involving Re, Ru, and Rh, which are mainly used as catalytic materials. Although most of these systems do not form compounds, our results still indicate that some structures are stable. Some of these stable structures are likely to be found only at certain temperatures; therefore, they can be considered to elicit the discovery of new materials. Although structures cannot be formed at room temperature, they can exist on the nanoscale, especially in the case of nanocatalysts. To design efficient nanocatalysts, all the possible theoretical structures should be considered.

1.2.2 Electronic information

Our aim is to create a database that contains complete electronic data, such as band structures and bandgap, for all existing compounds. This is a challenging project

that is still ongoing. A first milestone already achieved is the selection and calculation of over 13,000 structures from over 200,000 ICSD compounds. The data generated would be available by accessing our user-friendly online database. A good example of an electronic structure is shown in Fig. 1.5.

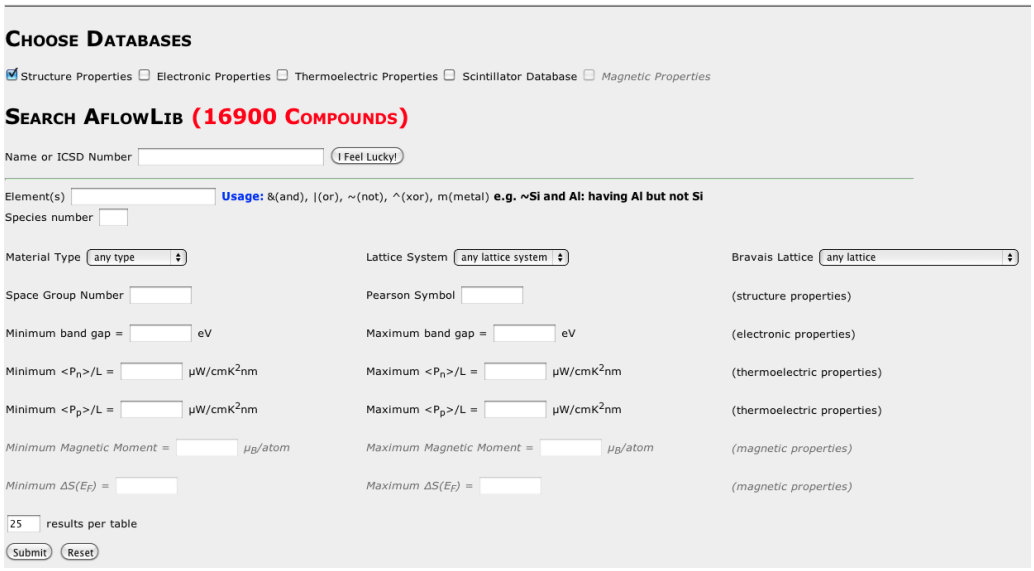

FIGURE 1.5: Screenshot of options.

For the online database, several options are available to narrow down the range of target materials. Some of the options are explained below:

1. **Choose Database**: Six optional databases are available, including databases of structure properties [Curtarolo et al. (2012a)], electronic properties [Setyawan et al. (2011)], thermoelectric properties [Fogden (1993)], scintillator properties [Levy et al. (2010b)], and magnetic properties. The additional option "Job Status" is reserved for future development.

2. **Name or ICSD number**: The user can access certain structures by directly entering their names in the alphabetical order (e.g., Al1Co2Mn1), their unique ICSD number (e.g., 57618), or even their unique ICSD label

(Al1Co2Mn1_ICSD_57618). If the results are available in the database, they are provided in the form of a table viewable in a web browser.

3. **Elements**: The user can select materials by combining elements with logical operators such as "and" (&), "or" (|), "not" (∼), and "xor" (∧). In addition, an extra option "metal" (m) is available. For example, the user can enter "Al & Co & m ∼ Mn" to select all possible materials that are metals containing aluminum, cobalt without manganese, and any other elements.

4. **Species Number**: With this option, the user can limit the number of elements from which the material may be made. For example, entering "3" for this option limits the search to only ternary compounds.

5. **Materials type**: This option has only two choices: metal or nonmetal (insulator or semiconductor).

6. **Lattice system**: Narrows the result to one of seven lattice systems.

7. **Bravais lattice**: The user can choose one of fourteen Bravais lattices as the constraint.

8. **Space group**: The user can restrict the space group for the structures to one of 230 possible space groups.

9. **Pearson symbol**: Select structures with certain Pearson symbols.

10. **Band gap**: Only materials falling into a specified bandgap range are shown in the result table. The user supplies the maximum and minimum bandgap values to determine the range. The default range is determined by the maximum and minimum values for our materials database.

11. **n-type or p-type**: This option is for the power factor.

12. **AFLOW version**: Data can be searched by the AFLOW version.

13. **Result per page**: The default value is 40 entries per page.

For example, by searching with element "Al" and three species in three databases, the result table would normally appear as shown in Figs. 1.6, 1.7, and 1.8. In addition, the user can obtain detailed information by clicking a name listed in the table. Clicking on a compound name given in the result table brings up the webpage for that compound through a permanent universal resource locator (url). For convenience, the unique url for each entry has already been created and is stored on our server. Figs. 1.10 and 1.11 show the normal format of each compound entry for $Ag_1Al_1O_2$_ICSD_95662. This page gives information on the lattice (number of atoms per cell, lattice type, superlattice, and symmetry operations including point group and space group), reciprocal lattice, and electronic properties. Furthermore, we not only provide the data for the compound but also generate graphical data, such as a dynamic three-dimensional lattice, Brillouin-zone figure, and band-structure figure. The data provided is consistent with *ab initio* calculations.

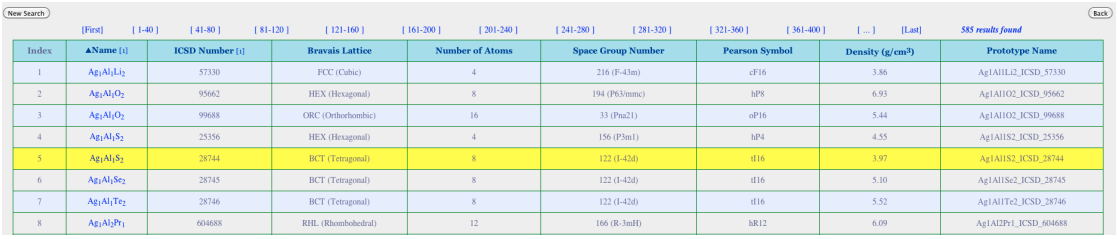
New Search

[First] [1-40] [41-80] [81-120] [121-160] [161-200] [201-240] [241-280] [281-320] [321-360] [361-400] [...] [Last] *585 results found*

Back

Index	▲Name [±]	ICSD Number [±]	Bravais Lattice	Number of Atoms	Space Group Number	Pearson Symbol	Density (g/cm³)	Prototype Name
1	$Ag_1Al_1Li_2$	57330	FCC (Cubic)	4	216 (F-43m)	cF16	3.86	Ag1Al1Li2_ICSD_57330
2	$Ag_1Al_1O_2$	95662	HEX (Hexagonal)	8	194 (P63/mmc)	hP8	6.93	Ag1Al1O2_ICSD_95662
3	$Ag_1Al_1O_2$	99688	ORC (Orthorhombic)	16	33 (Pna21)	oP16	5.44	Ag1Al1O2_ICSD_99688
4	$Ag_1Al_1S_2$	25356	HEX (Hexagonal)	4	156 (P3m1)	hP4	4.55	Ag1Al1S2_ICSD_25356
5	$Ag_1Al_1S_2$	28744	BCT (Tetragonal)	8	122 (I-42d)	tI16	3.97	Ag1Al1S2_ICSD_28744
6	$Ag_1Al_1Se_2$	28745	BCT (Tetragonal)	8	122 (I-42d)	tI16	5.10	Ag1Al1Se2_ICSD_28745
7	$Ag_1Al_1Te_2$	28746	BCT (Tetragonal)	8	122 (I-42d)	tI16	5.52	Ag1Al1Te2_ICSD_28746
8	$Ag_1Al_2Pr_1$	604688	RHL (Rhombohedral)	12	166 (R-3mH)	hR12	6.09	Ag1Al2Pr1_ICSD_604688

FIGURE 1.6: Result table from structure database. The table contains the compound name, unique ICSD number, Bravais-lattice type, number of atoms per primitive cell, space group number, Pearson symbol, density, and prototype.

1.2.3 Magnetic properties

ICSD is not the only database; the system also offers the Heusler magnetic database. This database is built by combining the Heusler, inverse Heusler, half-Heusler, and

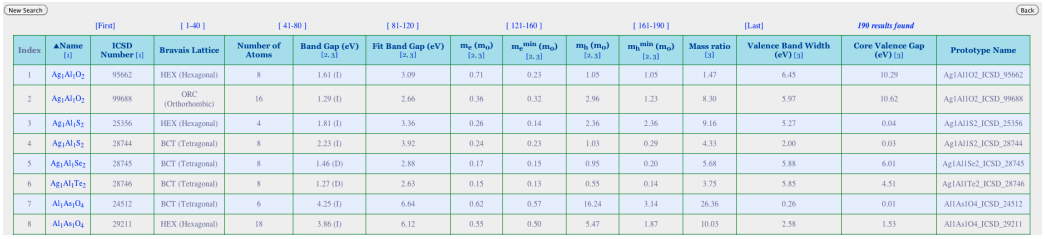

New Search | Back

[First] [1-40] [41-80] [81-120] [121-160] [161-190] [Last] *190 results found*

Index	▲Name [1]	ICSD Number [1]	Bravais Lattice	Number of Atoms	Band Gap (eV) [2, 3]	Fit Band Gap (eV) [2, 3]	m_e (m_0) [2, 3]	m_e^{min} (m_0) [2, 3]	m_h (m_0) [2, 3]	m_h^{min} (m_0) [2, 3]	Mass ratio [3]	Valence Band Width (eV) [3]	Core Valence Gap (eV) [3]	Prototype Name
1	$Ag_1Al_1O_2$	95662	HEX (Hexagonal)	8	1.61 (I)	3.09	0.71	0.23	1.05	1.05	1.47	6.45	10.29	Ag1Al1O2_ICSD_95662
2	$Ag_1Al_1O_2$	99688	ORC (Orthorhombic)	16	1.29 (I)	2.66	0.36	0.32	2.96	1.23	8.30	5.97	10.62	Ag1Al1O2_ICSD_99688
3	$Ag_1Al_1S_2$	25356	HEX (Hexagonal)	4	1.81 (I)	3.36	0.26	0.14	2.36	2.36	9.16	5.27	0.04	Ag1Al1S2_ICSD_25356
4	$Ag_1Al_1S_2$	28744	BCT (Tetragonal)	8	2.23 (I)	3.92	0.24	0.23	1.03	0.29	4.33	2.00	0.03	Ag1Al1S2_ICSD_28744
5	$Ag_1Al_1Se_2$	28745	BCT (Tetragonal)	8	1.46 (D)	2.88	0.17	0.15	0.95	0.20	5.68	5.88	6.01	Ag1Al1Se2_ICSD_28745
6	$Ag_1Al_1Te_2$	28746	BCT (Tetragonal)	8	1.27 (D)	2.63	0.15	0.13	0.55	0.14	3.75	5.85	4.51	Ag1Al1Te2_ICSD_28746
7	$Al_1As_1O_4$	24512	BCT (Tetragonal)	6	4.25 (I)	6.64	0.62	0.57	16.24	3.14	26.36	0.26	0.01	Al1As1O4_ICSD_24512
8	$Al_1As_1O_4$	29211	HEX (Hexagonal)	18	3.86 (I)	6.12	0.55	0.50	5.47	1.87	10.03	2.58	1.53	Al1As1O4_ICSD_29211

FIGURE 1.7: Result table from electronic properties database. The table contains the compound name, unique ICSD number, Bravais-lattice type, number of atoms per primitive cell, bandgap, fitted bandgap, effective mass of electrons and related parameters, mismatch mass ratio, valence-band width, core bandgap, and prototype.

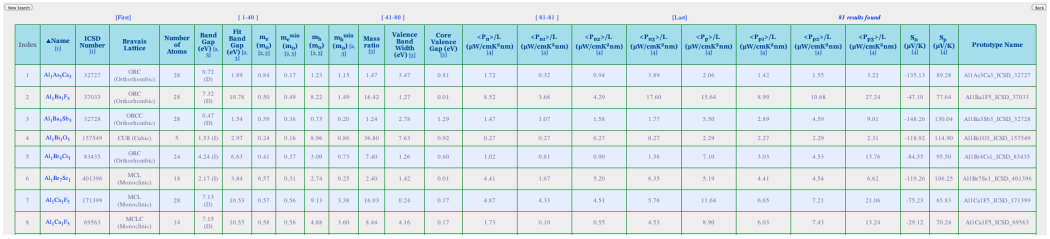

New Search | Back

[First] [1-40] [41-80] [81-81] [Last] *81 results found*

Index	▲Name [1]	ICSD Number [1]	Bravais Lattice	Number of Atoms	Band Gap (eV) [2, 3]	Fit Band Gap (eV) [2, 3]	m_e (m_0) [2, 3]	m_e^{min} (m_0) [2, 3]	m_h (m_0) [2, 3]	m_h^{min} (m_0) [2, 3]	Mass ratio [3]	Valence Band Width (eV) [3]	Core Valence Gap (eV) [3]	$<P_{xx}>/L$ (μW/cmK²nm) [4]	$<P_{xy}>/L$ (μW/cmK²nm) [4]	$<P_{xz}>/L$ (μW/cmK²nm) [4]	$<P_{yy}>/L$ (μW/cmK²nm) [4]	$<P_{yz}>/L$ (μW/cmK²nm) [4]	$<P_{zz}>/L$ (μW/cmK²nm) [4]	$<P_{zz}>/L$ (μW/cmK²nm) [4]	S_{xx} (μV/K) [4]	S_{yy} (μV/K) [4]	Prototype Name
1	$Al_1As_1Ca_1$	32727	ORC (Orthorhombic)	28	0.72 (D)	1.89	0.84	0.17	1.23	1.15	1.47	3.47	0.81	1.72	0.32	0.94	3.89	2.06	1.42	1.55	3.22	-135.13	89.28	Al1As1Ca1_ICSD_32727
2	$Al_1Ba_1F_5$	37033	ORC (Orthorhombic)	28	7.32 (D)	10.78	0.50	0.49	8.22	1.49	16.42	1.27	0.01	8.52	3.66	4.29	17.60	15.64	8.99	10.68	27.24	-47.10	77.64	Al1Ba1F5_ICSD_37033
3	$Al_1Ba_1Sb_3$	32728	ORCC (Orthorhombic)	28	0.47 (D)	1.54	0.59	0.36	0.73	0.20	1.24	2.78	1.29	1.47	1.07	1.58	1.77	5.50	2.89	4.59	9.01	-148.26	130.04	Al1Ba1Sb3_ICSD_32728
4	$Al_1Bi_1O_3$	157549	CUB (Cubic)	5	1.53 (I)	2.97	0.24	0.16	8.96	0.86	36.80	7.63	0.92	0.27	0.27	0.27	0.27	2.29	2.27	2.29	2.31	-118.92	114.90	Al1Bi1O3_ICSD_157549
5	$Al_1Br_4Cs_1$	83435	ORC (Orthorhombic)	24	4.24 (I)	6.63	0.41	0.37	3.00	0.73	7.40	1.26	0.60	1.02	0.81	0.90	1.36	7.10	3.03	4.53	13.76	-84.55	95.50	Al1Br4Cs1_ICSD_83435
6	$Al_1Br_3Sr_1$	401396	MCL (Monoclinic)	18	2.17 (I)	3.84	6.57	0.31	2.74	0.25	2.40	1.42	0.01	4.41	1.67	5.20	6.35	5.19	4.41	4.54	6.62	-119.26	106.25	Al1Br3Sr1_ICSD_401396
7	$Al_1Ca_1F_5$	171399	MCL (Monoclinic)	28	7.13 (D)	10.53	0.57	0.56	9.13	3.38	16.03	0.24	0.17	4.87	4.33	4.51	5.76	11.64	6.65	7.21	21.06	-75.23	85.83	Al1Ca1F5_ICSD_171399
8	$Al_1Ca_1F_5$	69563	MCLC (Monoclinic)	14	7.15 (D)	10.55	0.58	0.56	4.88	3.60	8.44	4.16	0.17	1.73	0.10	0.55	4.53	8.90	6.03	7.43	13.24	-29.12	70.24	Al1Ca1F5_ICSD_69563

FIGURE 1.8: Result table from thermoelectric database. The table contains the power factor, Seeback coefficient, and all the data from the electronic properties database.

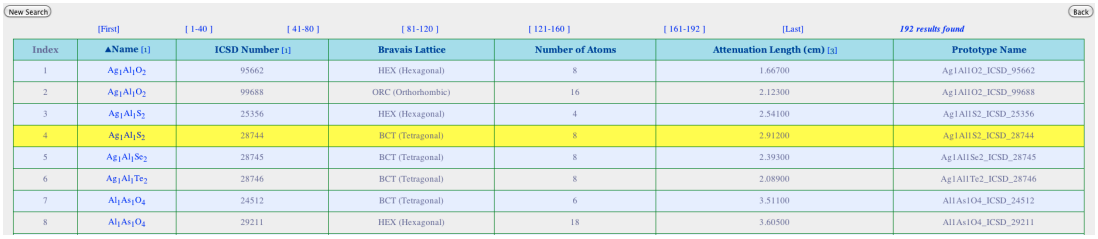

New Search | Back

[First] [1-40] [41-80] [81-120] [121-160] [161-192] [Last] *192 results found*

Index	▲Name [1]	ICSD Number [1]	Bravais Lattice	Number of Atoms	Attenuation Length (cm) [3]	Prototype Name
1	$Ag_1Al_1O_2$	95662	HEX (Hexagonal)	8	1.66700	Ag1Al1O2_ICSD_95662
2	$Ag_1Al_1O_2$	99688	ORC (Orthorhombic)	16	2.12300	Ag1Al1O2_ICSD_99688
3	$Ag_1Al_1S_2$	25356	HEX (Hexagonal)	4	2.54100	Ag1Al1S2_ICSD_25356
4	$Ag_1Al_1S_2$	28744	BCT (Tetragonal)	8	2.91200	Ag1Al1S2_ICSD_28744
5	$Ag_1Al_1Se_2$	28745	BCT (Tetragonal)	8	2.39300	Ag1Al1Se2_ICSD_28745
6	$Ag_1Al_1Te_2$	28746	BCT (Tetragonal)	8	2.08900	Ag1Al1Te2_ICSD_28746
7	$Al_1As_1O_4$	24512	BCT (Tetragonal)	6	3.51100	Al1As1O4_ICSD_24512
8	$Al_1As_1O_4$	29211	HEX (Hexagonal)	18	3.60500	Al1As1O4_ICSD_29211

FIGURE 1.9: Result table from scintillator database. The table contains the attenuation length and structure parameters.

30 elements that have a high probability to form magnetic materials, as determined by *ab initio* calculations. Its selection constraints are different from those offered through the website.

1. **Prototype**: The default setting for this option selects all structures from which the database is constructed, except that only Heusler, inverse-Heusler,

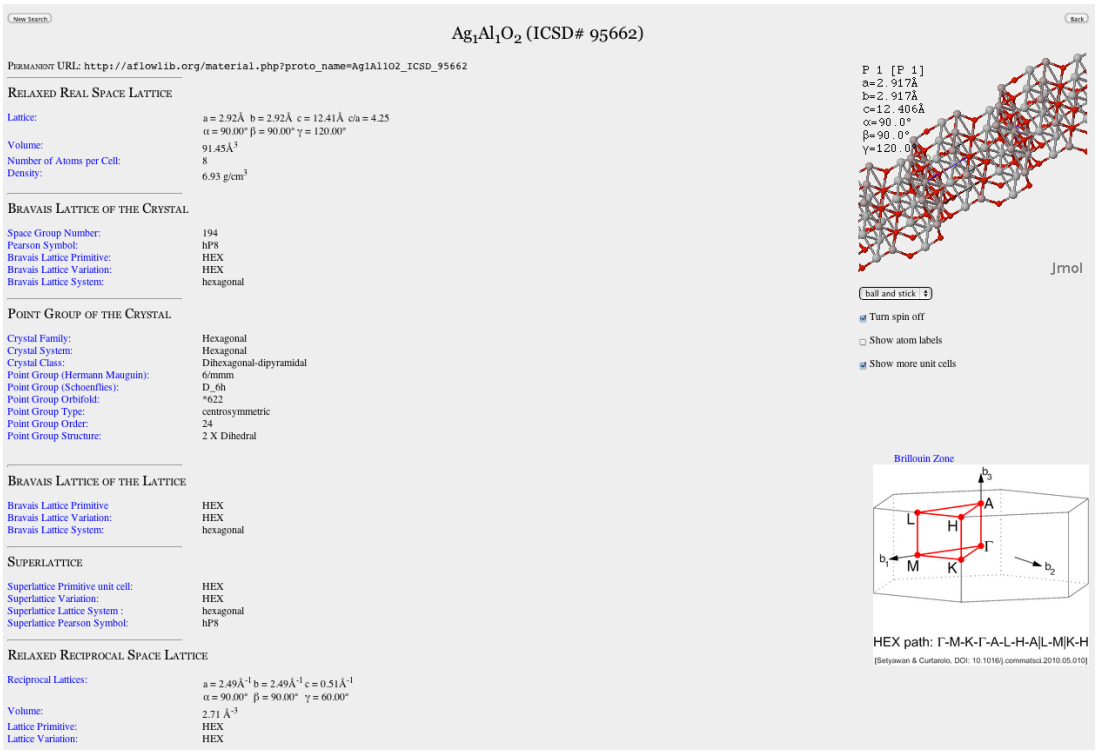

FIGURE 1.10: Structure-information entry for $Ag_1Al_1O_2$.

or half-Heusler structures may be chosen.

2. **Bandgap**: This is the same as the ICSD bandgap. The user can enter the bandgap range to constrain the search for materials.

3. **Bandgap type**: The database search can be constrained by three types of bandgaps: metal, direct bandgap, and indirect bandgap.

4. **Magnetic moment**: This option is similar to the bandgap option and is used to constrain the range of magnetic moment per atom of materials.

5. ΔS_{E_F}: ΔS_{E_F} represents the spin polarization at the Fermi level. Setting this option constrains the result to materials within this boundary.

These options allow the user to easily target materials with the desired properties from our online database. After submission and with the multiple constraints set,

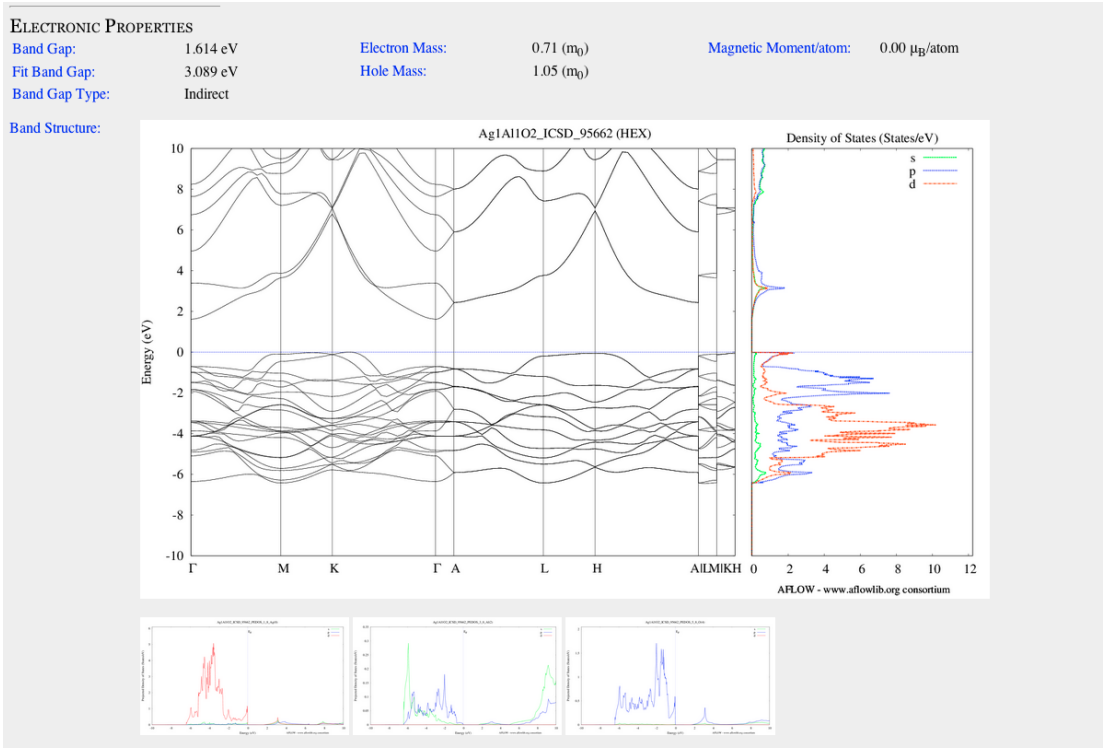

FIGURE 1.11: Electronic-information entry for $Ag_1Al_1O_2$.

AFLOW generates a result table that differs from an ICSD-generated result table. The AFLOW result table lists the compound name, prototype, volume, magnetic moment related, bandgap, bandgap type, spin polarization at the Fermi level, and spin decomposition. These table entries are explained below:

1. **Name**: This column gives the common compound name for each structure, such as $Al_2Co_1Mn_1$.

2. **Proto type**: This column indicates where the structure comes from. There are three prototypes: Heusler ($AlCu_2Mn$), inverse Heusler ($CuLi_2Sn$), and half-Heusler (AgAsMg).

3. **Volume**: This column gives the volume of the primitive cell.

4. μ, μ/**atom,** μ/**V**: The quantity μ is the magnetic moment for the given cell. The natural unit for magnetic moment is the Bohr magneton (μ_B).The quantity μ/atom is the magnetic moment per atom and μ/V is the magnetic moment per volume.

5. **Spin decomposition**: The spin decomposition is the magnetic dipole moment projected onto each atom.

In addition to these parameters, the table also gives the bandgap, bandgap type, and other information similar to what is listed on the ICSD-generated result table. By using this user-friendly online database, we can scan the entire database to extract materials with the desired physical constants. To demonstrate an application, we use our database to investigate spintronics, which is introduced in chapter 4.

1.3 Discovery of advanced materials

The materials database constructed with AFLOW has been applied to several research areas. In this section, we report results achieved with topological insulators, thermo-electric materials, and alloy systems.

A topological insulator is an insulator within its bulk but a conductor on its surface. A recent study [Hasan and Kane (2010)] shows that the main search strategy for topological insulators consists of observing their electronic structure and strong spin-orbit coupling properties. In AFLOW, the electronic structures of compounds are automatically generated by calculating the structures of compounds from the ICSD [Karen and Hellenbrandt (2002); Brown et al. (2005); Belsky et al. (2002)]. Furthermore, to improve the accuracy, AFLOW can calculate the spin-orbit coupling for the selected structures.

Thermo-electrical materials provide another example. The best thermo-electrics are those with the maximum figure of merit (ZT) [Snyder and Toberer (2008)].

AFLOW calculates the electronic structures and extracts the related parameters, such as the Seeback coefficient (S), the electrical conductivity (σ), and the thermal conductivity (κ). These are used to determine the figure of merit (ZT) (Eq. 1.1), which is the primary parameter. The quantity ZT can be systematically obtained from AFLOW calculations as follows:

$$ZT = \frac{\sigma S^2 T}{\kappa}. \tag{1.1}$$

Spintronics applications involve devices that exploit the interplay between the solid state environment and particle spin [Žutić et al. (2004)]. A half-metal [Eschrig et al. (2003); Pickett and Moodera (2001)] is a material that acts as an insulator for one spin direction but as a conductor for the opposite spin direction; half-metals have potential applications in spintronics. Our group has created a magnetic properties database for discovering half-metals. The database focuses on ternary structures and Heusler structures because we believe compounds with such structures are most likely to become half-metals.

For half-metals, the essential parameter that is checked is the spin polarization at the Fermi level (ΔS_{E_F}),which is given by Eq. (1.2). In this equation, N_+ is the total number of spin-up (and N_- is the total number of spin-down) particles. We use the trapezoidal rule to numerically integrate the number of spin-up and spin-down particles for ΔS_{E_F}. Detailed information on this topic is presented in Chapter 4.

$$\Delta S_{E_F} = \frac{N_+ - N_-}{N_+ + N_-} \tag{1.2}$$

2

Structure Prototypes

2.1 Introduction

An enormous number of known crystal structures have been discovered and the quantity of these structures is steadily growing. In order to gain insight into the relationships between patterns and mechanisms in configurations of crystal structures, we proposed to design a systematic approach to crystal structure classification. The basic principal in the classification of crystal structures is the *crystal prototype*—an abstraction of the crystal system by differentiating crystal structure with respect to geometry and symmetry. The crystal prototype is one of a crystal group with the same atomic density in primitive cell, the same Bravais lattice type, the same atomic environment and the same coordinates of each atom. This approach offers an effective path for selecting materials with specific properties in a first and general prediction quickly and accurately. A large number of structure properties, from different compounds, can be explored and deduced by comparison from similar structures [Curtarolo et al. (2003)].

A prototype database, from structures of compounds in the Inorganic Crystal

Structures Database (ICSD) [Mighell and Karen (1993); Karen and Hellenbrandt (2002); Brown et al. (2005); Belsky et al. (2002)] evaluated by high-throughput (HT) quantum mechanical calculations, has been created. As an example of this method, the Pt-Ru (platinum-ruthenium) system can be considered. Two ostensibly equivalent structures (same Bravais lattice, Pearson symbol, and even space group) exist; however, each has a different ground state energy and magnetic energy. In conjunction with our HT framework AFLOW [Curtarolo et al. (2012b)], with our effective algorithms implemented into the program, we can easily classify these two structures into two different groups.

With our crystal structure prototype database, we can easily generate structures with diversity of species. Then, these theoretical created structures will be fully relaxed by our efficient tool, AFLOW. During this process, prototype classification will help the user to avoid redundant *ab initio* calculations. For instance, in the system AlCo, we have three compounds Al_1Co_1, Al_2Co_2 and Al_4Co_4. If we utilize these three compounds to construct our Al-Co alloy system, we need to calculate these three compounds respectly. In fact, these three structures share same structure pattern, which means only one of them should be calculated instead of all. To differentiate these patterns, prototype classification function will be loaded and generate a table of classification results. We will add the structures, which are unique and ground states after relaxation, to our prototype database. Then we can establish alloy systems with these unique structures without any repeated calculations.

2.2 Prototype classification method

In past decades, space group and Bravais lattice type usually were utilized as crystal structure classification methods. Space group and Bravais lattice type both represent the crystal structures for long-range order. In fact, two structures have same space group or Bravais lattice type may have different structures with distinct ground state

energies. On the other hand, Daams [Daams et al. (1992)] has mentioned short-range order is a dominant factor for intermetallic properties. Based on this theory, we apply both short-range and long-range orders as constraints to classification, which improves the accuracy of materials selections for specific properties.

For crystal systems classification, the general algorithm performs as follows. Several constraints have been applied for calculating geometry of different compounds. These include Bravais lattice type, Pearson symbol, point group of crystal pattern, factor group, the site symmetries of corresponding atoms and atomic environment. From this starting point, we compare two different compounds restricted by these constraints. Then we can differentiate whether two atomic configurations are equivalent or not. Furthermore, we can scan all the compiled ICSD, comparing each structure versus existing prototypes, to establish prototype classified database. With this classified database, we can get the compounds with similar structures and ground states quickly.

Following are the steps for comparison of two structures:

1. Geometrical parameters initialization.
2. Primitive cell standardization of crystal structures.
3. Structures comparison with several constraints
4. Prototype output

These four steps will be explained in details in the following sections.

2.2.1 Geometrical parameters initialization

Geometrical parameters are the data describing where the atoms are located and what the coordinate system of crystal structure is. With these parameters, we generate the geometrical input file. To be consistent with future work, we use the input

format from Vienna *ab initio* Simulation Package (VASP) for first principal calculation. This geometrical file called a POSCAR, which contains compound name, lattice vectors, coordinates of atoms and species of atoms.

The geometrical file is written in several lines:

1. Name of compound or comment.
2. Universal scaling factor or the total volume of cell, if it is negative.
3. Lattice vectors a_1, a_2, a_3.
4. Numbers of atoms for different elements, which are same order listed from line 8.
5. Selective dynamics which decide to choose Cartesian coordinates and fractional coordinates along the lattice vectors.
6. Coordinates of each atom with respect to the element.

Following is the geometrical input file for AuMg. Line one is the title for this compound. In the second line, the positive number is a scaling factor. Then there are three lattice vectors in the next three consecutive lines. For the sixth line, the numbers of atoms with respect to different species are listed. At last, those parameters are the fractional coordinates and the species name of each atom.

```
1  AuMg/120 - (120) - HCP [A2B2] (120)  (htqc library)
2  -82.016400
3    1.00000000000000   0.00000000000000   0.00000000000000
4    0.00000000000000   0.00000000000000   1.63299316185545
5    0.00000000000000  -1.73205080756888   0.00000000000000
6  2 2
```

```
7  Direct(4) [A2B2]
8      0.00000000000000    0.00000000000000    0.00000000000000  Au
9      0.00000000000000    0.50000000000000    0.33333333333333  Au
10     0.50000000000000    0.00000000000000    0.50000000000000  Mg
11     0.50000000000000    0.50000000000000    0.83333333333333  Mg
```

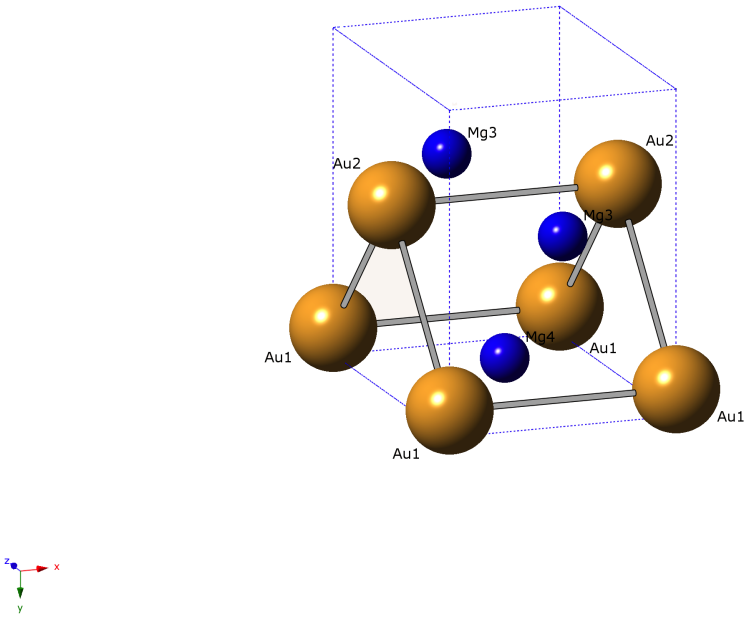

FIGURE 2.1: Original primitive cell for AuMg.

2.2.2 Primitive cell standardization

Starting from geometrical input files, our efficient tool, AFLOW, will be used to calculate the structure symmetries and extract the standardized forms of crystal structures. Without a standardized form, crystal structures comparison are not amenable to compare coordinates.

The principal of standardizing primitive cell is to determine possible translational vectors, which are the vectors starting from one atom site and ending in another,

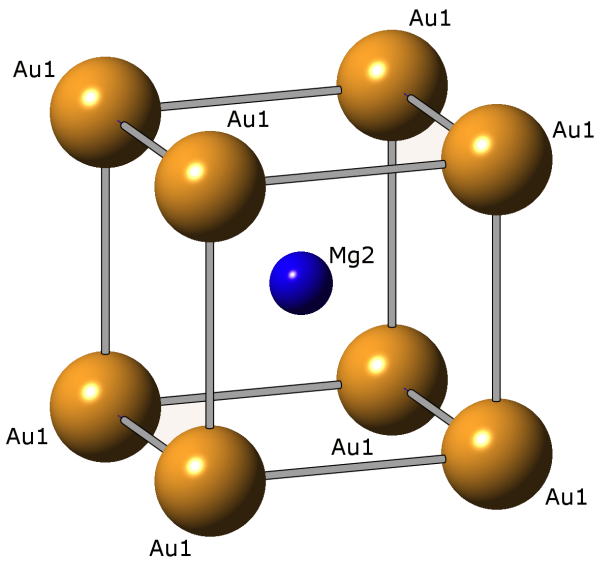

FIGURE 2.2: Standardized primitive cell for AuMg.

as potential lattice vectors. We scan all the possible vectors to find the ones with the intersection angle close to 90 degree. Figure (2.1) is the original primitive cell. With our primitive cell standardizing, the primitive cell has been transformed into a new coordinates system (Fig 2.2). This process provides us an easy path to clarify normal structure from different observations.

2.2.3 Structures comparison with constraints

For this new data after standardization, we store the structure data in the program, which contains space group with symmetry operations and translational operations, point group with symmetry operations, Bravais lattice type, Pearson symbol and atomic coordinates both in fractional and Cartesian coordinate systems.

In the following step, the first comparison is made with atomic density in one primitive cell for two selected structures. The reason for simply comparing the atomic density in primitive cell is that atoms in one of primitive cell cannot map to another

one, which has different numbers of atoms in primitive cell. If the numbers are same, the program continues to compare the lattice type of structures. In this operation, we believe two structures will have same prototype, if their Bravais lattice types are the same, because the Bravais lattice type definition is based on atomic sites, which are the patterns that similar structures will have. Then we could differentiate the crystal structures into 14 groups of Bravais lattice types. Thus, the comparison is accelerated by using this classification.

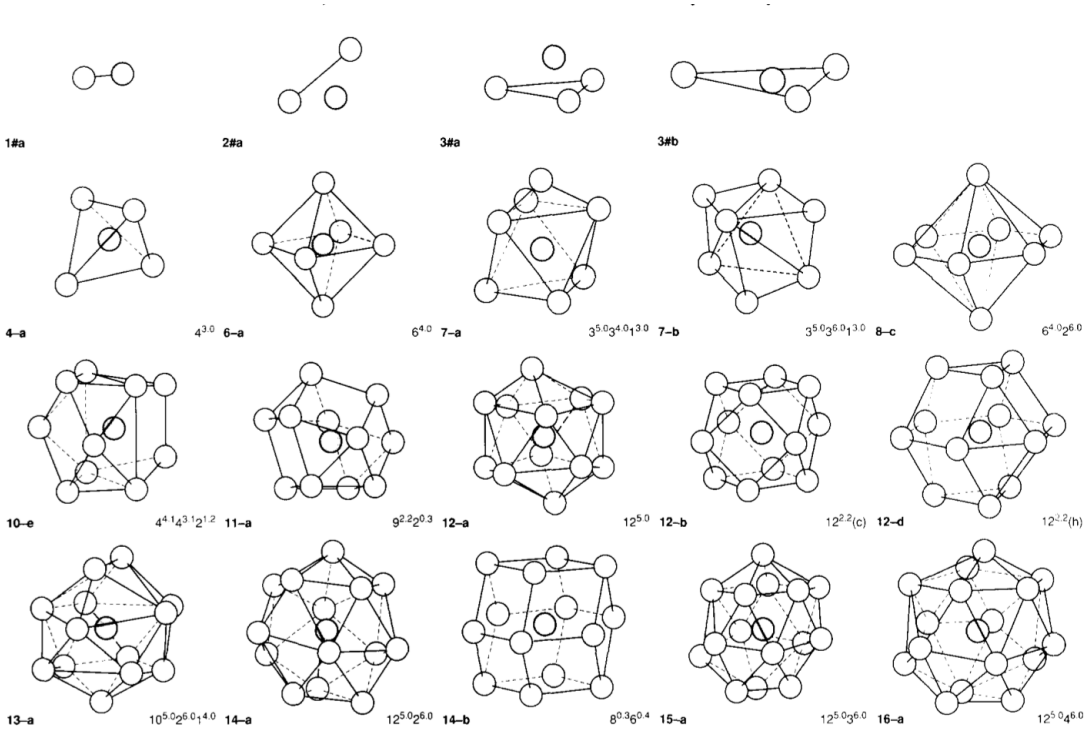

FIGURE 2.3: 14 common patterns of atomic environment types [Villars and Daams (1993)]. Reprinted with permission from Elsevier.

Atomic environment [Daams et al. (1992)] comparison follows the Bravais lattice type differentiating. Comparison for atomic environment is supported by the idea that short-range order is the dominant factor, which may affect materials intermetallic properties [Bever (1985)]. Thus, this selection constraint is a reasonable approach to improve classification accuracy. We first move the origin to an atom and cal-

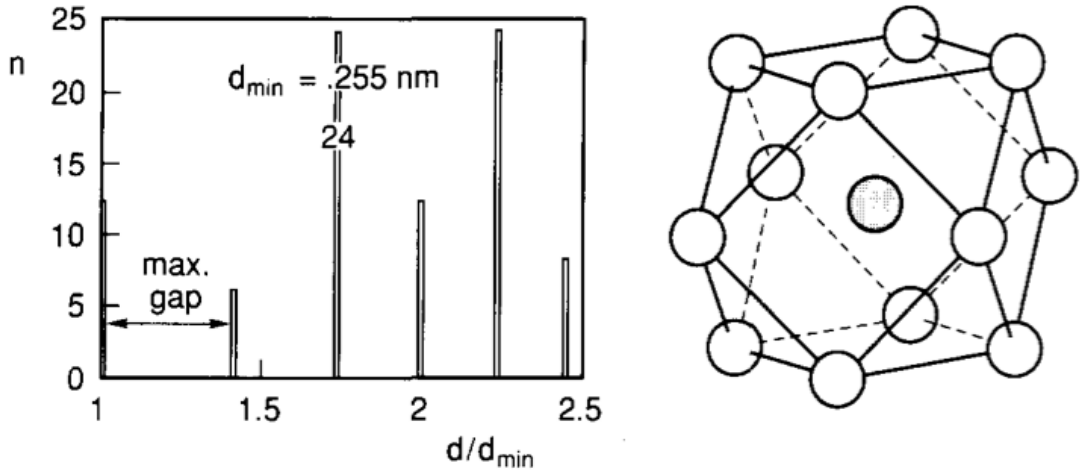

FIGURE 2.4: Atomic environment histogram and visualized into polyhedron for cubooctahedron [Villars and Daams (1993)]. Reprinted with permission from Elsevier.

culate the relative distance between origin and other atoms. Subsequently, we can plot the histogram of distances by the maximum-gap rule [Brunner (1971)]. This histogram can be used to formulate atomic environment polyhedrons. There are 14 patterns of atomic environment types, which represent almost 80 percents of all the configurations (Fig.2.3) [Villars and Daams (1993)]. Figure (2.4) shows an example of a histogram and an atomic environment polyhedron of cubooctahedron. The cubooctahedron is the atomic environment polyhedron for face centered cubic Bravais lattice cell. Every corner is occupied by one atom. The nearest neighbor atoms form the first shell. The number of atoms in different shells are proportional to the height of bars in the histogram. As the example of cubooctahedron, the first shell contains 12 atoms. Furthermore, this histogram and polyhedron structure are translated into numerical data. What concerns us is the shell inside the maximum-gap that can be used to construct atomic environment polyhedron [Villars and Daams (1993)]. Then we compare the atomic environment using AFLOW.

Finally, an exact method for differentiating similar structures (same atomic envi-

ronment, same Bravais lattice type, same space group) is to calculate their relative distant s for atoms in two structures with respect to several certain symmetry operations and translational operations. With the fact that structures from experimental data are observed using different rules, same structures will have different atom sites. When the symmetry operations are applied to one of the structures, the result is a rotated or shifted set of atoms along the translational vectors, which could map the atoms to other coordinate systems.

2.3 Results of classification

This efficient tool has been implemented into AFLOW. It has two different functions. The first function is to classify several structures into different unknown group. The first selected structure for that group will be the group prototype. Furthermore, the other function is base on our classification of ICSD database and proto structures [Curtarolo et al. (2005)]. We use the classified database to search the existed compounds in ICSD or in our binary proto structure database. Table 2.1 provides the details of binary proto structures.

Table 2.1: Binary prototype table

Structure Number	Pearson symbol	Name	*Strukturbericht* symbols	PROTO	Space group
FCC					
1,2	fcc/cF4	$Fm\bar{3}m$	A1	Cu	225
1.cub,2.cub	fcc/cF4	$Fm\bar{3}m$	A1	Cu	225
3	tP2	P4/mmm	$L1_0$	AuCu	123
4	hR2	$R\bar{3}m$	$L1_1$	CuPt	166
5,6	tI6	I4/mmm	$\beta 1/2$	AB2	139
7,8	oI6	Immm	-	MoPt2	71
9,10	hP3	$P\bar{3}m1$	$\alpha 1/2$	AB2	164
11,12	oS8	Cmmm	$L1_3$	AB3	65
13,15	tP4	P4/mmm	Z1/3	AB3	123
14	tP4	P4/nmm	Z2	A2B2	129

continued ...

Structure Number	Pearson symbol	Name	*Strukturbericht* symbols	PROTO	Space group
16,18	mS8	C2/m	-	AB3	12
17	mS8	C2/m	W2	A2B2	12
19,21	oP4	Pmmm	Y1/3	AB3	47
20	oP4	Pmmm	Y2	A2B2	47
22,24	tI8	I4/mmm	$D0_{22}$	Al3Ti	139
23	tI8	I41/amd	CH"40"	NbP	141
25,26	cP4	Pm3$\bar{m}$	$L1_2$	AuCu3	221
27,29	hR4	R$\bar{3}$m	V1/3	AB3	166
28	hR4	R$\bar{3}$m	V2	A2B2	166
BCC					
58,59	bcc/cI2	Im$\bar{3}$m	A2	W	229
58.cub,59.cub	bcc/cI2	Im$\bar{3}$m	A2	W	229
60	oS4	Cmmm	-	γ-IrV	65
61	cP2	Pm$\bar{3}$m	B2	CsCl	221
62,63	hP3	P$\bar{3}$m1	-	AB2	164
64,65	oF12	Fmmm	-	AB2	69
66,67	tI6	I4/mmm	$C11_b$	MoSi2	139
68,69	hR4	R$\bar{3}$m	-	AB3	166
70,72	oS8	Cmmm	-	AB3	65
71	oS8	Cmma	-	A2B2	67
73,75	mP4	P2/m	-	AB3	10
74	mP4	P21/m	-	A2B2	11
76,78	tP4	P4/mmm	-	AB3	123
77	tP4	P4/nmm	B11	γ-CuTi	129
79,81	oI8	Immm	-	AB3	71
80	oI8	Imma	-	A2B2	74
82,83	tP4	P4/mmm	$L6_0$	CuTi3	123
84,86	cF16	Fm$\bar{3}$m	$D0_3$	AlFe3/BiF3	225
85	cF16	Fd$\bar{3}$m	B32	NaTl	227
HCP					
115,117	hcp/hcp2	$P6_3$/mmc	A3	Mg	194
116	hP2	P_6m2	B_h	WC	187
118,121	oP4	Pmm2	-	AB3	25
119	oP4	Pmmn	-	CuTe	59
120	oP4	Pmma	B19	AuCd	51
123	oI8	C2/m	-	A2B2	12
122,124	oI8	Imm2	-	AB3	44
125,127	hP4	P$\bar{6}$m2	-	AB3	187
126	hP4	P$\bar{3}$m1	-	A2B2	164
128,132	mS12	Cm	-	AB5	8

continued ...

Structure Number	Pearson symbol	Name	*Strukturbericht* symbols	PROTO	Space group
129,134	mS12	C2/m	-	A4B2	12
130,137	mS12	C2/m	-	A4B2	12
131,135	mS12	C2/m	-	A4B2	12
133,140	mS12	Cm	-	A2B4	8
136	mS12	Cm	-	A3B3	8
138,139	mS12	Cm	-	A3B3	8
141,145	oS12	Amm2	-	AB5	38
142,147	oS12	Cmcm	-	A4B2	63
143,150	oS12	Cmcm	-	A4B2	63
*144,148	oS12	Cmcm	-	A4B2	63
*146,153	oS12	Amm2	-	A2B4	38
*149,151	oS12	Amm2	-	A3B3	38
*152,157	oS12	Amm2	-	A3B3	38
*154,160	hP6	$P\bar{6}2m$	-	AB5	189
*155,158	hP6	$P\bar{6}2m$	-	A2B4	189
*156,159	hP6	Cmcm	-	A2B4	63
*161,167	hR6	R32	-	AB5	155
*162,165	hR6	R32	-	A2B4	155
*163,166	hR6	C2/c	-	A2B4	15
*164	hR6	C2	-	A3B3	5
*168,169	hP6	$P\bar{6}m2$	-	AB5	187
*170,175	hP6	$P\bar{6}m2$	-	A2B4	187
*172	mS8	$P\bar{6}m2$	-	A3B3	187
*171,176	hP6	$P\bar{3}m1$	-	A2B4	164
*173,177	hP6	P63/mmc	-	A2B4	194
*174	hP6	P3m1	-	A3B3	156
178,179	hP12	$P6_3/mm$	C14	MgZn2	194
180,181	oP16	Pnma	$D0_{11}$	Fe3C	62
182,183	cF24	$Fd\bar{3}m$	C15	Cu2Mg	227
184,185	cP8	Pm3(bar)n	A15	Cr3Si	223
186,187	hP8	$P6_3/mmc$	$D0_{19}$	Ni3Sn	194
188,189	oS12	Cmcm	C49	ZrSi2	63
190,191	hP3	P3m1	ω phase with Z=1/4	-	164
192,193	oC8	Cmcm	$B33B_f$	CrB	63
194	oS8	Cmcm	-	ITl	63
195	cP8	$P2_13$	B20	FeSi	198
196,197	tP4	P4/nmm	O2	-	CdTi
198	oP24	Pbcm	-	InTh	57
199	tI16	I4/mcm	B37	SeTl	140
201	cF8	$Fm\bar{3}m$	B1	NaCl	225

continued ...

Structure Number	Pearson symbol	Name	*Strukturbericht* symbols	PROTO	Space group
202,203	tI10	I4/mmm	$D1_3$	BaAl4	139
204,205	hP6	P6/mmm	$D2_d$	CaCu5	191
206,207	tI26	I4/mmm	$D2_b$	ThMn12	139
208,209	hP9	$P\bar{6}2m$	C22	Fe2P	189
210,211	oP12	Pnma	C37	Co2Si	62
212,213	hR19	-	-	Th2Zn17	166
214,215	cI28	$I\bar{4}3d$	$D7_3$	Th3P4	220
216,217	hP3	P6/mmm	C32	AlB2	191
218	cF8	$F\bar{4}3m$	B3	ZnS	216
219	hP4	P63/mc	B4	ZnS	186
220,221	hP4	P63/mmc	$B8_1$	NiAs	194
222,223	hP16	P63/mcm	$D8_8$	Mn5Si3	193
224,225	hP38	P63/mmc	-	Th2Ni17	194
226,227	cP8	$Pm\bar{3}n$	A15	Cr3Si	223
228,229	tP6	P4/nmm	C38	Cu2Sb	129
230,231	tI12	-	C16	CuAl2	140
232,233	tI6	I4/mmm	$C11_b$	MoSi2	139
234,235	tl12	I4/mcm	C16	Al2Cu	140
236,237	cl184	$Im\bar{3}$	Cd6Y	(Y12Cd68)	204
238,239	hp24	$P\bar{6}m2$	-	Co3V	187
238,239	hp24	P63/mmc	Pu3Al	-	194
***240,241	-	P42/mnm	$D8_b$	CrFe	136
242,243	oP24	PmnmO2	-	NbPd3	59
244,245	-	P63/mmc	$D0_{24}$	Ni3Ti	194
246,247	hP6	P63/mmc	-	CaIn2	194
248,249	tI12	I41/amd	C_c	ThSi2	141
***250,251	tI6	I4/mmm	$C11_a$	CaC2	139
252,253	cF24	$F\bar{4}3m$	$C15_b$	AuBe5	216
254,255	tI32	I4/mcm	-	W5Si3	140
254,255	hP5	P63/mmc	$D5_2$	La2O3	194
256	oP8	Pnma	B27	BFe	62
257,258	oP6	Pnnm	C18	FeS2	58
259,260	hR5	$R\bar{3}m$	C33	Bi2Te3	166
261,262	cF96	$Fd\bar{3}m$	-	Ti2Ni	227
263,264	tI14	I4/mmm	-	Ti3Cu4	139
265,266	tP10	-	-	Ti2Cu3	129
267,268	oP6	Pnnm	C18	FeS2	52
269,270	hP3	$P\bar{3}m1$	C6	CdI2	164
271,272	oC16	Cmcm	-	YCd3	63
273,274	hP6	P63/mmc	$B8_2$	Ni2In	194

continued ...

Structure Number	Pearson symbol	Name	*Strukturbericht* symbols	PROTO	Space group
275,276	hP6	P63/m	-	Ni2Si	176
277,278	oP8	PmmnO1	$D0_a$	βCu3Ti	59
279,280	tI16	I4/mmm	$D0_{23}$	Al3Zr	139
281,282	cP12	$Pa\bar{3}$	C2	FeS2	205
283,284	oI12	Imma	-	GdSi2(1.4)	74
285,286	tI10	I4/m	$D1_a$	MoNi4	87
287,288	tI6	I4/mmm	-	CuZr2	139
289,290	cP4	$Pm\bar{3}m$	$D0_9$	αReO3	221
291,292	tP4	P4/nmm	B10	PbO/PbS	129
301,302	cF8	$Fd\bar{3}m$	A4	C	(DIA)
303,304	tI2	I4/mmm	A6	Indium	139
305,306	tI4	I41/amd	A5	βSn	141
307,308	hR6	$R\bar{3}m$	A7	αAs	166
309,310	cF32	$Fm\bar{3}m$	-	CuPt7	225
311,312	tI18	I4/mmm	-	NbNi8	139
313,314	tI18	I4/mmm	-	V4Zn5	139
315,316	hP24	$P6_3/mmc$	C36	MgNi2	194
317,318	oC8	Cmca	A11	αGa	64
319,320	cI58	$I(\bar{4})3m$	A12	αMn	217
321,322	cP20	$P4_132$	A13	βMn	213
323,324	hP3	$P3_21\bar{D}^6_3$	A8	γSe	152
325,326	hP4	P63/mmc	A9	graphite	194
327,328	tI2	I4/mmm	Aa	αPa	139
329,330	tP30	$P4_2/mnm$	Ab	βU	136
331,332	oP8	I4/mmm	Ac	αNp	62
333,334	tP4	P4/nmm	Ad	βNp	129
335,336	hP1	P6/mmm	Af	hex	$HgSn_{6-10}$
337,338 todo	-	Ag	T-50 boron	-	
339,340 todo	-	Ah	simple cubic	-	
341,342 todo	-	Ai	βPo	-	
343,344 todo	-	Ak	αSe	-	
345,346 todo	-	Al	βSe	-	
347,348 todo	-	A3′	αLa	-	
349,350	hR1	$R\bar{3}m$	A10	αHg	166
351,352 todo	-	A14	In2	-	
353,354 todo	-	A16	αS	-	
355,356 todo	-	A17	black	-	
357,358 todo	-	A20	αU	-	
359,360	hP18	P63/mcm	-	Ga4Ti5	193
361,362	tP20	P42/mnm	-	Al2Zr3	136

continued ...

Structure Number	Pearson symbol	Name	*Strukturbericht* symbols	PROTO	Space group
363,364	hP7	P6/mmm	-	Al3Zr4	191
365,366	oF40	F2dd	-	Al3Zr2	43
367,368	cF112	$Fm\bar{3}c$	-	NaZn13	226
369,370	cP7	$Pm\bar{3}m$	-	CaB6	221
371,372	hP5	$P\bar{3}m1$	$D5_{19}$	Al3Ni2	164
373,374	cI40	$I\bar{4}3m$	-	Ga4Ni(Ga3.62Ni0.97)	217
375,376	oC16	Cmmm	-	Ga3Pt5	65
377,378	mS44	C12/m1	-	Ga9Ni13	12
379,380	cI112	$Ia(\bar{3})d$	-	Ga4Ni3	230
381,382	tI24	$I4_1/amd$	-	Ga2Hf	141
383,384	cF116	$Fm\bar{m}$	-	C6Mn23	225
385,386	oP44	Pnma	-	Cu8Hf3	62
387,388	oS68	Cmca	-	Ni10Zr7	64
389,390	tP3	P4/mmm	-	Hg2Pt	123
391,392	oP20	Pnma	-	B4Mg	62
393,394	oI64	Imma	-	B7Mg	74
395,396	oP16	Pbam	-	Ge3Rh5	55
397,398	tP14	P4/mbm	-	In4Ti3	127
399,400	tP34	P4/nmm.O2	V8Sb9	V7.49Sb9	129
401,402	tI160	$I\bar{4}2d$	-	Li3B14	122
403,404	tP20	Pa/mbm	-	LiB3	127
405,406	hR4	$R\bar{3}m$	-	LiB-MS1	166
407,408	hP8	P63/mmc	-	LiB-MS2	194
411,412	cI58	$I\bar{4}3m$	-	Re24Ti5	217
413,414	mS36	C12/m1	-	Ni7Zr2	12
415,416	tI40	I4/m	-	Pt11Zr9	87
417,418	oP20	Pnma	-	Au4Zr	62
419,420	oI142	Immm	-	Hf54Os17	71
421,422	hP9	$P6_222$	C40	CrSi2	180
423.424.t0	hP68	P6/m	-	Ag51Gd14.o3.t0	175
423.424.t1	hP68	P6/m	-	Ag51Gd14.o3.t1	175
423.424.t2	hP68	P6/m	-	Ag51Gd14.o3.t2	175
423,424.t3	hP68	P6/m	-	Ag51Gd14.o2.t3	175
423,424.t4	hP68	P6/m	-	Ag51Gd14.o2.t4	175
423,424.t5	hP68	P6/m	-	Ag51Gd14.o2.t5	175
423,424.t6	hP68	P6/m	-	Ag51Gd14.o2.t6	175
423,424.t7	hP68	P6/m	-	Ag51Gd14.o1.t7	175
423,424.t8	hP68	P6/m	-	Ag51Gd14.o1.t8	175
423,424.t9	hP68	P6/m	-	Ag51Gd14.o1.t9	175
425,426	cF184	$Fd\bar{3}m$	-	Zn22Zr	227

continued ...

Structure Number	Pearson symbol	Name	*Strukturbericht* symbols	PROTO	Space group
427,428	oP24	Pnnm	-	As2Ti	58
429,430	tI84	I4/mmm	-	Ge10Ho11	139
431,432	hP48	$P6_122$	-	Ir3Zr5	178
433,434	oP6	Pnnm	-	CaCl2	58
435,436	cP5	$P\bar{4}3m$	-	CFe4	215
437,438	mS28	C12/c1	-	C2Mn5	15
439,440	oP40	Pnma	-	C3Mn7	62
441,442	hP20	$P6_3mc$	-	Fe3Th7	186
443,444	hR24	$R\bar{3}cr$	-	F3Fe	167
445,446	hR24	P321	-	F3Fe	150
447,448	mP4	$P12_1/m1$	-	NiTi	11
449,450	cP6	$Pn\bar{3}m$	C3	Ag2O	224
451,452	hP9	$P\bar{3}$	Bb	etaAg2Zn	147
453,454	mC16	C2/m	$D0_{15}$	AlCl3	12
455,456	hR8	R32	$D0_{14}$	AlF3	155
457,458	hR10	$R\bar{3}c$	$D5_1$	αAl2O3	167
459,460	cI26	$Im\bar{3}$	-	Al12W	204
461,462	oP12	P212121	-	Ag2Se	19
463,464	hR26	$R\bar{3}$	-	AlPd	148
465,466	cP16	$Pa\bar{3}$	SC16	AlSb	205
467,468	cI52	$I\bar{4}3m$	γBrass	Cu5Zn8	217
469,470	hR36	$R\bar{3}m$	h	-	BaPb3
471,472	hP8	Cmcm	-	Hf3Sc*-h321	63
473,474	hP6	$P\bar{6}2m$	-	Hf5Sc-h51	189
475,476	mC12	C2/m	-	BiHf2-134	12
477,478	tP6	P4/mmm	-	Hf5Pb-f63	123
479,480	oC12	Cmmm	-	HfPd5	65
481,482	hR276	$R\bar{3}ch$	-	Re25Zr21	167.2
483,484	tP6	P4/mmm	$B11_3$	-	123
485,486	tP6	P4mm	$B11_{3'}$	-	99
487,488	tP6	P4/mmm	Z3	-	123
489,490	tP6	P4mm	Z3'	-	99
491,492	oP102	$Pmn2_1$	Al13Co4	-	31
493,494	ms102	C1m1	Al12.13Co4	eta	8
495,496	hP28	$P6_3/mmc$	Al5Co2	-	194
497,498	mp22	$P12_1/c1$	Al9Co2	-	14
499,500	tP10	$P\bar{4}2_1c$	-	Pd4Se	114
501,502	cF1192	$Fd(\bar{3})m$	-	NaCd2	227
503,504	hP10	$P6_3/m$	-	Er3Ru2	176
505,506	oP40	Pnma	-	Pt3Sr7	62

continued ...

Structure Number	Pearson symbol	Name	*Strukturbericht* symbols	PROTO	Space group
507,508	cF120	$Fm\bar{3}m$	-	Ir4Sc11	225
509,510	oP276	Pnna	-	Ru25Y44	52
511,512	cP252	$P4_132$	-	RuZn6	213
513,514	mP4	P21/m	B19'	NbRu-β"	11
515,516	cF96	$Fd\bar{3}m$	-	δCdNi	227.2
517,518	hP3	$P\bar{3}m1$	-	Cd2Ce	164
519,520	hP3	P6/mmm	-	Hg2U	191
521,522	hP9	$P\bar{6}2m$	-	InMg2	189
523,524	oS16	Cmcm	-	Cd3Er	63
525,526	hP8	$P6_3/mmc$	-	CdMg3	194
527,528	hP24	$P6_3/mmc$	-	CeNi3	194
529,530	oP32	Pnma	-	CoSc3	62
531,532	tP4	P4/mmm	-	Pb3Sr	123
533,534	hR36	$R\bar{3}mh$	-	PuNi3	166
535,536	oP16	Pnma	-	YZn3	62
537,538	hR4	$R\bar{3}m$	-	Co2Y2*	166
539,540	mS12	C2/m	-	Sc2Zr*	12
541,542	oI8	Immm	-	Mo3Ti*-81	71
543,544	oI8	Imma	-	MoTi*-80	74
545,546	hR3	$P\bar{3}m1$	-	ReTi2*-81	164
547,548	tI6	I4/mmm	-	Hf2Tl*-6	139
549,550	oF12	Fmmm	-	Be2Zn*-65	69
551,552	oI8	Imm2	-	Re3Ru*-124	44
553,554	hP24	P63cm	$D0_{21}$	Cu2.82P	185
555,556	oP108	Pnma	-	Mg2Au	62
557,558	cF16	$Fm\bar{3}m$	-	BiF3	225
559,560	cI58	$I\bar{4}3m$	-	Al12Mg17	217
561,562	oS160	Cmcm	-	MgAu3-x	63
563,564	oS64	Cmcm	-	MgAu3+x	63
565,566	oF48	Fddd	-	Mg2Cu	70
567,568	hP18	$P\bar{6}2c$	-	Mg2Ga	190
569,570	oP24	Pbam	-	MgGa2	55
571,572	oI28	Ibam	-	Mg5Ga2	72
573,574	tI28	I4/mmm	-	Mg2Ga5	139
575,576	tI32	I41/a	-	MgGa	88
577,578	hR72/24	R32	-	Mg3Hg	155
579,580	hR48/16	$R\bar{3}m$	-	Mg3In	166
581,582	cF408	$F\bar{4}3m$	-	Mg44Rh7	216
583,584	cF12	$Fm\bar{3}m$	-	CaF2	225
585,586	hP8	P63/mmc	$D0_{18}$	Al3Ir	194

continued ...

Structure Number	Pearson symbol	Name	*Strukturbericht* symbols	PROTO	Space group
587,588	cF116	$Fm\bar{3}m$	-	Mn23Th6	225
589,590	cP39	$Pm\bar{3}$	-	Mg2Zn11	200
591,592	mS110	C2/m	-	Mg4Zn7	12
593,594	cP20	$P4_132$	-	Mg3Ru2	213
595,596	oS12	Cmcm	-	Au2V	63
597,598	hP94	P63/mmc	-	Sr9Mg38	194
600.ABCDE	tP30	$P4_2/mnm$	σ	CrFe	136
611,612	cP140	$Pm\bar{3}$	-	Rh13Sc57	200
613,614	hR13	Imm2	-	Fe7W6	166
615,616	oP24	Pbca	-	AuSn2	61
617,618	mS12	C2./m	-	Bi2Pd	12
619,620	mS28	C2./m	-	Bi2Pd5	12
621,622	oP16	Pnma	-	Bi3Ni	62
623,624	oP32	Pnma	-	Bi3Y5	62
625,626	cI120	$Ia\bar{3}d$	-	Bi4Rh	230
627,628	hR48	$R\bar{3}m$	-	BiMn3	166
629,630	oP16	Pmma	-	BiPd3	51
631,632	tI12	I4/mmm	-	BiTi2	139
633,634	mP12	$P2_1./c$	-	CoSb2	14
635,636	hR78	R3m	-	Cu7Hg6	160
637,638	oI12	Imma	-	Hg2K	74
639,640	cI52	$I\bar{4}3m$	-	Ir2Zn11	217
641,642	tI32	$I\bar{4}$	$D0_e$	Ni3P	82
643.AB/BA	aP32	$P\bar{1}$	-	KP15	2
644.AB/BA	tI116	$I4_1/a$	-	Pu28Zr	88
645.AB/BA	cF52	$Fm\bar{3}m$	B12U	-	225
646.AB/BA	oS68	Cmcm	TiZn16	-	63
647.AB/BA	tI140	I4/mcm	Rh2Y3	-	140
648.AB/BA	tP32	P4/ncc	Rh3Pu5	-	130
649.AB/BA	tI32	$I\bar{4}2m$	α-SV3	-	121
650.AB	oP12	Pmma	-	IrTa	51
651.AB/BA	oP36	Pnma	-	Ge4Sm5	62
652.AB/BA	oP12	Pnma	-	Cl2Pb	62
653.AB/BA	mP16	$P12_1$	-	NbPt3	11
654.AB/BA	cI10	$Im\bar{3}m$	-	Hg4Pt	229
655.AB/BA	hR14	$R\bar{3}$	-	Pd4Pu3	148
656.AB/BA	hR15	$R\bar{3}$	-	Er3Ni2	148
657.AB/BA	oI6	Immm	-	Pd2Ti	71
658.AB/BA	tP8	P4/mmm	-	Pd5Ti3	123

continued ...

Structure Number	Pearson symbol	Name	*Strukturbericht* symbols	PROTO	Space group
659.AB/BA	oS20	Cmcm	-	Pd3Ti2	63
660.AB/BA	tP14	P4/mbm	-	Hg5Mn2	127

```
    TYPE            NUM OF ATOMS        PEARSON        BRAVAIS              NAME                        LABEL
       1                     3,1            cI8            BCC             Ag1Te3                      Ag1Te3
                             3,1            cI8            BCC             Au1Sb3                      Au1Sb3
                             3,1            cI8            BCC              Si1W3                       Si1W3
POSCAR:
Ag1Te3 #160.2 - (Ag1Te3_ICSD_37186) - Ag1Te3 [Ag1Te3] hR4 R3mH AgTe3 160 Ag1Te3_ICSD_37186 ICSD_37186  (icsd library)
 (WICKOFF 160.2 #160) (sg.opt flipped)  [BCC,BCC,cI8] (STD_PRIM doi:10.1016/j.commatsci.2010.05.010)  [BCC,BCC,cI8]
(STD_PRIM doi:10.1016/j.commatsci.2010.05.010)#Ag1Te3_ICSD_37186
-113.74
-3.0522e+00  3.0522e+00  3.0522e+00
 3.0522e+00 -3.0522e+00  3.0522e+00
 3.0522e+00  3.0522e+00 -3.0522e+00
1 3
Direct(4)
 0.0000e+00  0.0000e+00  0.0000e+00 A
 5.0850e-01  6.9000e-03  5.0850e-01 B
 5.0850e-01  5.0850e-01  6.9000e-03 B
 6.9000e-03  5.0850e-01  5.0850e-01 B
5.28663 5.28663 5.28663 109.471 109.471 109.471 -113.74

Atomic Environment:
6,6,6,6


       2                   16,10           cI52            BCC              Ag5Cd8                      Ag5Cd8
POSCAR:
Ag5Cd8 #217 - (Ag5Cd8_ICSD_604897) - Ag5Cd8 [Ag5Cd8] cI52 I-43m Ag5Cd8 217 Ag5Cd8_ICSD_604897 ICSD_604897  (icsd library)
 (WICKOFF 217 #217)  [BCC,BCC,cI52] (STD_PRIM doi:10.1016/j.commatsci.2010.05.010)  [BCC,BCC,cI52]
(STD_PRIM doi:10.1016/j.commatsci.2010.05.010)  [BCC,BCC,cI52] (STD_PRIM doi:10.1016/j.commatsci.2010.05.010)#Ag5Cd8_ICSD_604897
-497.38
-4.9912e+00  4.9912e+00  4.9912e+00
 4.9912e+00 -4.9912e+00  4.9912e+00
 4.9912e+00  4.9912e+00 -4.9912e+00
10 16
Direct(26)
 0.0000e+00  6.5000e-01  0.0000e+00 A
 3.5000e-01  3.5000e-01  3.5000e-01 A
 6.5000e-01  0.0000e+00  0.0000e+00 A
 0.0000e+00  0.0000e+00  6.5000e-01 A
 0.0000e+00  3.5800e-01  3.5800e-01 A
 0.0000e+00  6.4200e-01  6.4200e-01 A
 3.5800e-01  3.5800e-01  0.0000e+00 A
 6.4200e-01  6.4200e-01  0.0000e+00 A
 6.4200e-01  0.0000e+00  6.4200e-01 A
 3.5800e-01  0.0000e+00  3.5800e-01 A
 0.0000e+00  2.1000e-01  0.0000e+00 B
 7.9000e-01  7.9000e-01  7.9000e-01 B
 2.1000e-01  0.0000e+00  0.0000e+00 B
 0.0000e+00  0.0000e+00  2.1000e-01 B
 2.7200e-01  6.2000e-01  2.7200e-01 B
 6.5200e-01  3.8000e-01  6.5200e-01 B
 3.4800e-01  0.0000e+00  7.2800e-01 B
 7.2800e-01  0.0000e+00  3.4800e-01 B
 0.0000e+00  3.4800e-01  7.2800e-01 B
 0.0000e+00  7.2800e-01  3.4800e-01 B
 3.8000e-01  6.5200e-01  6.5200e-01 B
 6.2000e-01  2.7200e-01  2.7200e-01 B
 7.2800e-01  3.4800e-01  0.0000e+00 B
 3.4800e-01  7.2800e-01  0.0000e+00 B
 2.7200e-01  2.7200e-01  6.2000e-01 B
 6.5200e-01  6.5200e-01  3.8000e-01 B
8.6451 8.6451 8.6451 109.471 109.471 109.471 -497.38

Atomic Environment:
13,13,13,13,13,13,13,13,13,12,12,12,12,15,15,15,15,15,15,15,15,15,15,15
```

FIGURE 2.5: Table of classified prototypes

For the first function, we input the list of compounds and compare two of them at each step. After finishing all the comparisons, the result will be written into a file named "Classify.out" with structure parameters. Figure (2.5) shows an example of classification results. There is a group number that is counted at the beginning of this

group. The structure parameters are consistent with the geometrical input file below the group information. Furthermore, for convinience, the geometrical information of the first structure with the numerical atomic environment has been written beneath the group information. This format can systematically be read by our program for prototype searching purpose.

For the second function, this tool can be used for searching the prototype in binary alloy prototype database, ICSD or even the database we created ourselves to find the standard structure. This searching can be realized by initializing geometrical input file and comparing with the prototypes in the classified prototype database one by one. With the classification of binary alloy prototype database, redundant comparisons can be avoid and calculations will be speed up.

2.4 Conclusions

In summary, using the concept of prototype, an effective algorithm has been implemented into AFLOW for materials selection and design for different properties purposes. Firstly, geometrical parameters will be standardized before prototype comparison. With strong constriants on atomic density in unit cell, Bravais lattice type, Pearson symbol, atomic environment and coordinates matching, structures are accurately compared by our efficient algorithm. In addition, for application of this algorithm, it can be either utilized for a large number of unknown structures comparison, or for a prototype search in databases. With respect of that, these unknown structures will add to our prototype database. This functionality will be done automatically in the future.

3

Discovering new materials through phase diagrams

3.1 Introduction

The fast growth of society has increased the need to improve advanced materials for use in, for example, new catalysts for fuel cells, topological insulators, or thermoelectric devices. Although numerous materials have been discovered experimentally, optimized materials for specific purposes are still lacking. Currently, computational methods are mainly used for discovering new materials.

One computational method of discovery is to study the structural stability of different systems. We implemented a systematic algorithm in our high-throughput (HT) software that uses *ab initio* calculations to study materials properties and used our prototype database to construct possible structures for binary alloy systems, for example, ruthenium and technetium. Ruthenium is generally used in the electronics and chemical industries and is an important catalyst for fuel cells [Taniguchi et al. (2004)] made of a ruthenium-platinum alloys, which provide the desired electrical performance. Furthermore, the materials properties of ruthenium are exceptionally useful in plasma display panels and hard disk drives, and it has potential applica-

tions in diverse fields, such as preventing corrosion and improving the mechanical properties of alloys for turbine blades. In addition, ruthenium alloys can also be used in luxury products (e.g., fountain-pen nibs). Of the 28 binary systems of ruthenium alloys, 16 are listed as phase separating and 3 as disordered α phases. This leaves 9 miscible systems, which are located in groups IIIB, IVB, and VB of the periodic table (Fig. 3.3). Because technetium is the only radioactive transition element, it is used in nuclear fuels; its radioactivity limits its use in experiments. Thus, we find that only half of the 28 technetium-transition-metal binary systems are phase separating Villars et al. (2004)]. These non-compound-forming systems are in groups IB, IIB, VIIB, and VIIIB of the periodic table (Fig. 3.7). Paradoxically, there are still several binary systems that can form phases with technetium in these phase-separating groups, such as manganese, iron, and zinc. The remaining systems are reported to have phases. This incomplete information indicates that experimental studies are not sufficient for technetium binary systems. Therefore, computations are required and preferable to predict the nature of technetium-ruthenium binary systems.

3.2 Constructing convex hulls for phase diagrams

AFLOW is an efficient HT framework based on *ab initio* calculations. All data processed by AFLOW to analyze ruthenium systems come from VASP energy calculations (Kresse and Hafner (1993)). With exchange-correlation functions and projected augmented wave (PAW) pseudopotentials, we calculate the energies for various structures of each binary system at zero temperature and pressure without lattice vibrations and with spin polarization. The real free energies are usually substituted by the energies of effective ground states, which are calculated at zero temperature. Since previous works support this approximation [Levy et al. (2011, 2010a)], the ground states are determined by *ab initio* calculations. Therefore, in our investigations of phase diagrams, the energies are calculated at zero temperature and all

the crystal structures are completely relaxed via *ab initio* calculations. The calculation routine consists of finding all possible structures in our binary database (see Table 2.1) and relaxing the structures. In addition, we use our prototype routine to determine whether the relaxed structures are unique within the binary prototype database. The structures that are unique and are not in our database are inserted as new prototypes for future phase-diagram construction. We then combine these structures with those already found experimentally [Monkhorst and Pack (1976)]. In designing the software, we strove to balance the speed of calculation with the accuracy of the results. The system allows us to virtually mix the reported structures with the hypothesized structure to evaluate the miscibility and stability of different binary alloy systems with reasonable speed and precise conclusions. Fig. (3.1) illustrates the strategy of the research plan.

We introduce a path for searching the ground state using a diagram, called a convex hull, to determine the local minimum energies at low temperature. This convex hull contains the formation energies as a function of concentration. It is constructed by several lines that connect the lowest-energy-ordered phases for a binary system. The phases with energies higher than the iso-energy line can be formed by mixing the structures from each endpoint of this line. Therefore, structures with energies above the line are considered unstable. Consequently, this diagram gives the stability of the binary systems at zero temperature. Fig. (3.2) shows an example of a convex hull. The horizontal axis gives the concentration of niobium starting from unity (pure niobium) on the left to zero (pure platinum) on the right. The vertical axis gives the energy of each structure in microelectron volts (meV). This result for the niobium-platinum binary system reproduces the stable structures found experimentally [Baker et al. (1986)] and allows us to predict several stable structures that have not been reported. Although the zero-temperature approximation does not lead to the complete and real phase diagram, we find that the majority of our calculated

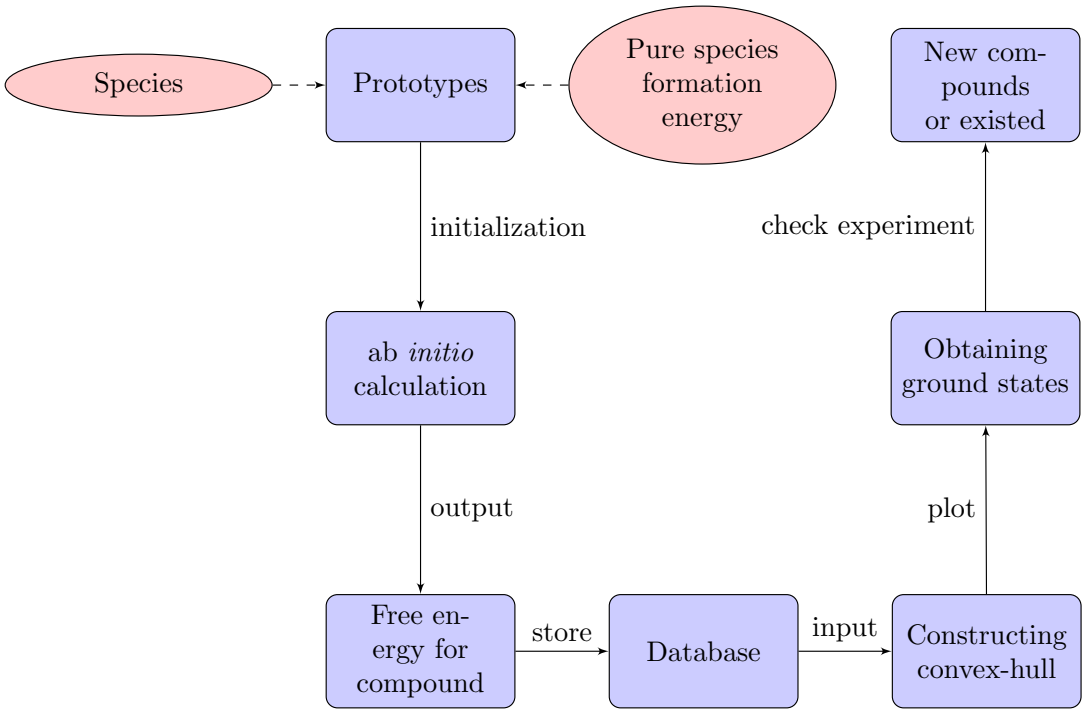

FIGURE 3.1: Phase-diagram research plan.

results are consistent with experimental data [Villars et al. (2004)] and predict unreported structures. In addition, ternary systems can be similarly analyzed, but the corresponding convex hull is extended to three dimensions. This algorithm will be integrated into AFLOW and the discussion of ternary systems is left for Chapter 4.

3.3 Ruthenium system

Ruthenium's catalytic properties are well known. It is used as a catalyst in solid oxide fuel cells. For this purpose, Pt-Ru-Ni and Pd-Ru alloys have been designed for direct

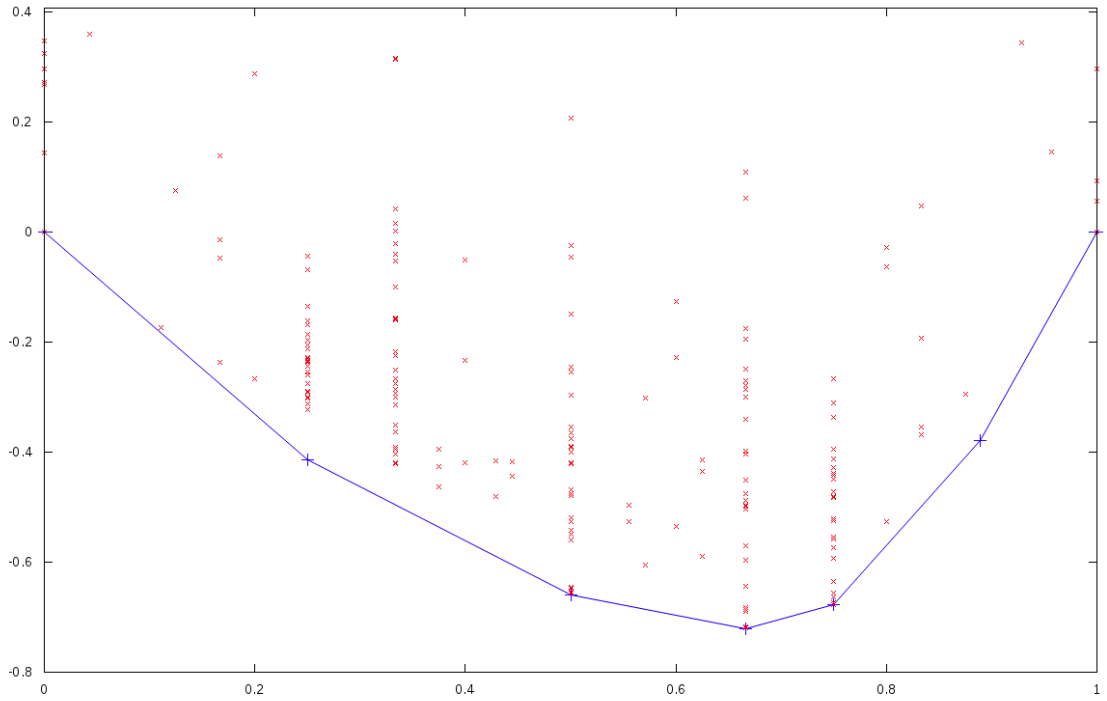

FIGURE 3.2: Nb-Pt binary convex hull.

methanol fuel cells [Bagchi and Bhattacharya (2008)] and ethanol alkaline fuel cells, respectively [Wang et al. (2010b); Prez et al. (2009)]. Furthermore, Pt-Ru alloys were found to be excellent catalysts that reduce the risk of carbon monoxide poisoning with respect to that of pure platinum [Okamoto (2004)]. In addition, they also serve as good substrates in the water dissociation reaction [Desai and Neurock (2003)]. Ru-Ni superalloys are another application of Ru. For this bimetallic compound, the Ru site occupation is the principal subject of investigation [40,41]. In the study of the Ru site, dislocation dynamics [Yu and Wang (2009)], interface strength [Gong et al. (2009); Wang and Wang (2008)], and elasticity [Bleskov et al. (2009)] are important topics. Ru-doped Nb-based superalloys are also good representations for Ru-based alloys, and several stable phases of Ru-Nb are shown to be shape-memory alloys [Shapiro et al. (2006); Tan et al. (2007); Benarchid et al. (2009); Mousa et al.

(2009)]. Finally, Ru substrates are also found to modify the growth of graphene [Peng and Ahuja (2010); Chen et al. (2010); Wang et al. (2010a); en Jiang et al. (2009)].

Combining thermodynamic theory and *ab initio* methods is useful for investigating ordered structures and stable compounds, especially in Mo-Ru systems [Kissavos et al. (2005); Shin et al. (2006); Kissavos et al. (2007); Grns et al. (2008)]. Experimental results should include a series of Ru alloys mixed at a high temperature. In previous work, $MoRu_3$ was found to be stable. Other phase-separating systems have also been explored, such as Ag-Ru, Co-Ru, Cu-Ru, Fe-Ru, Ni-Ru, Ru-Pd, and Ru-Ta [He et al. (2008); Spišák et al. (2001); He et al. (2007, 2006); Kong et al. (2005); Wang et al. (2006, 2009)]. The original computation methods are constrained by the physical models upon which they are based and the hardware upon which they are executed. As large data in materials science has become a hot topic, the development of HT methods has grown quickly. For large systems in materials science, HT methods are used for materials design and improvement [Curtarolo et al. (2005); Jóhannesson et al. (2002); Stucke and Crespi (2003); Curtarolo et al. (2003); Wang et al. (2011); Lewis et al. (2007); Ozolins et al. (2008); Ortiz et al. (2009); Setyawan and Curtarolo (2010); Setyawan et al. (2011)]. These efficient methods provide insights into trends in material properties and predict materials that have not yet been discovered experimentally.

In this section, we discuss calculations of Ru binary alloys that have been generated and run by our HT framework AFLOW. We analyze the stability of compounds by calculating the enthalpy of formation for possible structures of this binary system. We then use these formation enthalpies to construct the binary convex hulls described in the previous section. For Ru, data from experiments is incomplete. Among the 28 selected Ru binary alloy systems, 16 are phase separating and 3 are in the disordered α phase [Villars et al. (2004); Baker et al. (1986)]. Our HT results

are consistent with experimental results for 9 systems with stable compounds and predict as-yet unknown materials for five systems: NbRu, RuTa, RuTi, RuV, and RuZn. Furthermore, the vibrational properties of these systems have been calculated. Before executing the *ab initio* calculation, structure relaxation is performed by AFLOW. The energy tolerance in these calculations is less than that used for component pseudopotential. Thus, through accurate calculations, these results can prevent wrap errors and lower numerical errors. The structure is fully relaxed when the stress tensor components decrease to 0.01 GPa and forces on atoms are less than 10-2 meV/A.

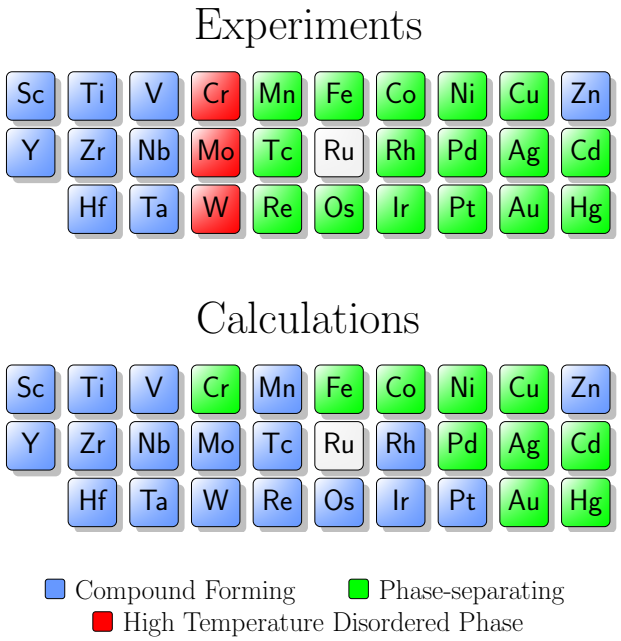

FIGURE 3.3: Ruthenium binary systems in the periodic table: phase-separating system (green), high-temperature disordered system (red), and miscible system (blue).

Table 3.1 presents the *ab initio* calculation and experimental results. The first column of the table is not ordered alphabetically but by the Mendeleev number [Pettifor (1984, 1986)]. The three middle columns represent the compounds determined experimentally [Villars et al. (2004); Baker et al. (1986)], by previous calculations

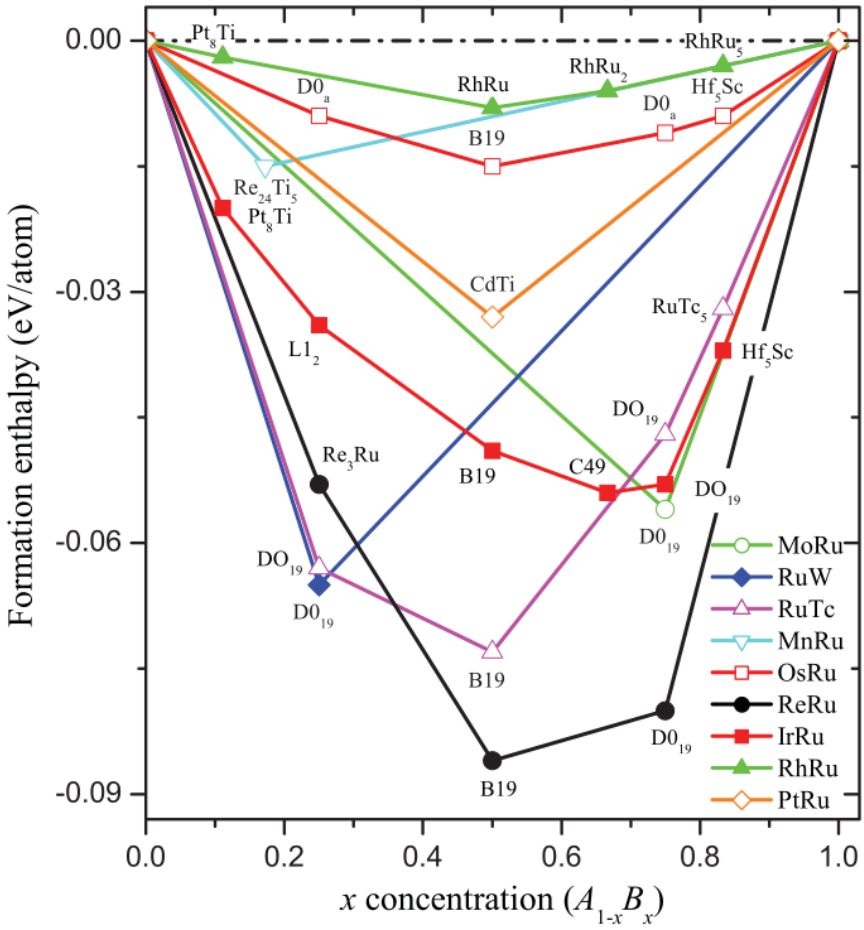

FIGURE 3.4: Convex hulls for ground states of systems that are noncompound-forming in experiments and that we predict to be miscible systems. From Jahnátek et al. (2011)

[Curtarolo et al. (2005)], and by our HT results. All data generated by our calculation is available through our **aflowlib.org** online database. These 28 systems can be classified into three clusters: the compound-forming phase, the high-temperature α phase, and the noncompound-forming phase. The order of these three clusters is the same as that in the table, except for the RuZn system. This system forms a stable compound but remains at the bottom of the table. From our calculations, we find that the majority of the systems from the top of the table to RuPt are compound-

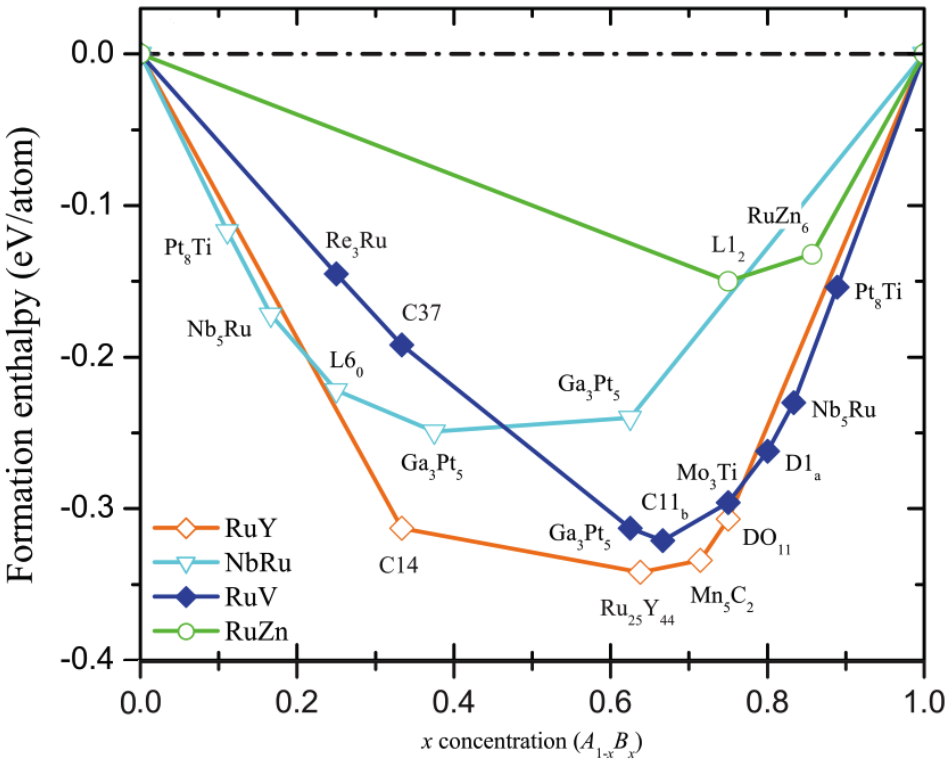

FIGURE 3.5: Convex hulls for Nb-Ru, Ru-V, Ru-Y, and Ru-Zn binary alloy systems. From Jahnátek et al. (2011)

forming systems. Only 4 of 21 systems are noncompound-forming. In these four system, CrRu is a disordered high-temperature α-phase system and the other three contain magnetic elements (cobalt, iron, and nickel). In the high-temperature α-phase cluster, there are three systems whose ground states are all bcc structures containing group-VIB elements. From our HT results, we find Ru_3X ($X =$ Mo or W) with prototype $D0_{19}$.

Based on experiments, 16 systems are noncompound-forming. Our HT calculations predict that seven of these systems could theoretically form stable phases (see Fig. 3.4). In particular, four ruthenium binary alloy systems with platinum groups are extremely important for chemical applications. IrRu, OsRu, and RhRu

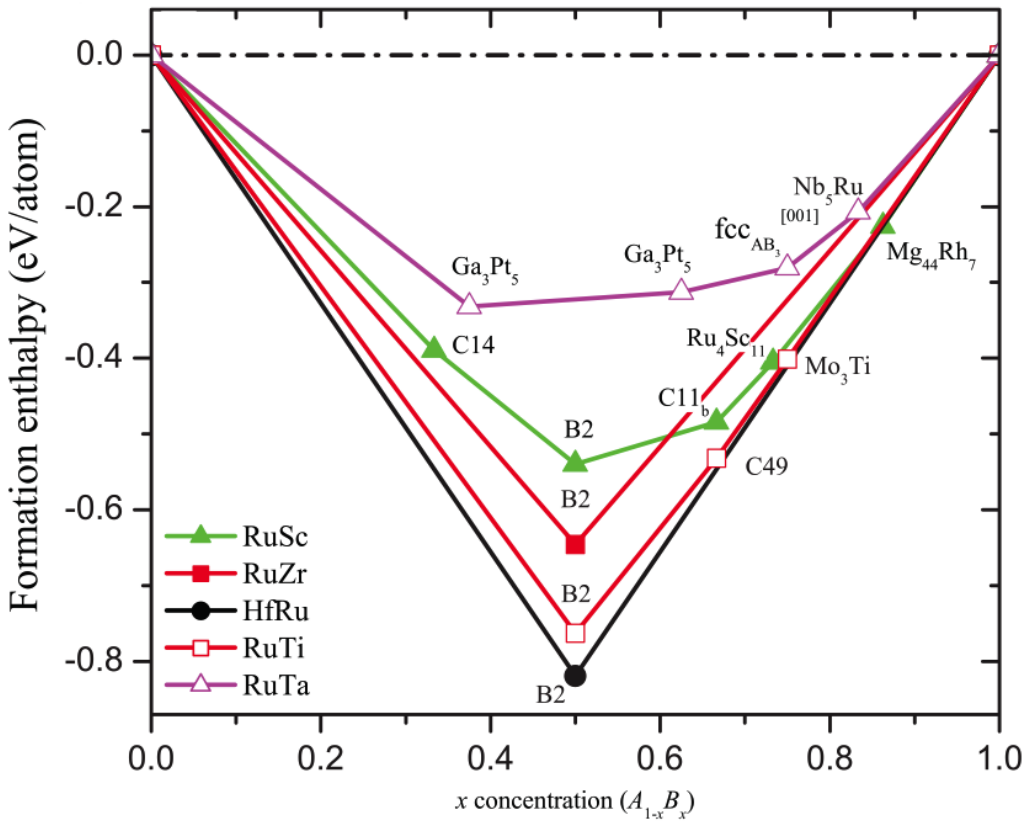

FIGURE 3.6: Convex hulls for Hf-Ru, Ru-Sc, Ru-Ta, Ru-Ti, and Ru-Zr binary alloy systems. From Jahnátek et al. (2011)

are predicted to have diverse ground states, and unique ground states only appear in PtRu with the CdTi prototype. Several ground states predicted by the HT method do not have a *Strukturbericht* designation or specified prototype. In Table 3.1, we use $*$ to label the ground states that have been discovered in former investigations [m65,88,89]. The symbol $\star$ in Table 3.1 represents the new prototype we explored, and detailed information on it is given in Table 3.2. The difference between previous work [Curtarolo et al. (2005)] and the current investigation is that to construct the binary systems, we used a large dataset of crystal structures. In Table 3.1, from PdRu to CdRu, the listed systems retain their phase-separating status.

Fortunately, our results are consistent with experimental results: the systems

we predict to be compound-forming have been discovered experimentally to have stable phases. Convex hulls, as described above, have been generated for these systems by AFLOW (see Figs. 3.5 and 3.6). For group-IIIB elements Y and Sc, our calculations closely reproduce the experimentally determined phase diagrams. On the basis of our calculations, the only difference is that Ru_3Sc_5 and Ru_2Y_3 do not form a stable phase at low temperature. An equi-atomic structure RuX emerges from experiments for the group-VB elements V, Nb, and Ta. In fact, because our calculations assume low temperature, they predict phase diagrams more complicated than those found experimentally and no stable RuX compounds. Thus, we generate much more information than that through experiments.

Table 3.1: The data obtained from experiments ("Exper.") or from HT calculations ("Calc.") for Ru binary alloys and formation enthalpies ("ΔH"). $*$ represents the prototypes in previous work. $\star$ labels the one is newly discovered and showed in Table 3.2. "N/A" denotes no data. "-" indicates no compound.

Element	Compounds			ΔH
	Exper.	Calc.(Previous)	Calc.(Present)	meV/atom
Y	Ru_2Y(C14)	Ru_2Y(C14)	Ru_2Y(C14)	-313
	$Ru_2Y_3(Er_3Ru_2)$			[79]
	$Ru_{25}Y_{44}(Ru_{25}Y_{44})$		$Ru_{25}Y_{44}(Ru_{25}Y_{44})$	-342
		RuY_2(C16)		[21]
	$Ru_2Y_5(Mn_5C_2)$		$Ru_2Y_5(Mn_5C_2)$	-334
	$RuY_3(D0_{11})$	$RuY_3(D0_{11})$	$RuY_3(D0_{11})$	-307
Sc	Ru_2Sc(C14)	N/A	Ru_2Sc(C14)	-389
	RuSc(B2)		RuSc(B2)	-540
	$Ru_3Sc_5(D8_8)$			[42]
	$RuSc_2(NiTi_2)$		$RuSc_2(C11_b)$	-484[84]
	$Ru_4Sc_{11}(Ir_4Sc_{11})$		$Ru_4Sc_{11}(Ir_4Sc_{11})$	-405
	$Ru_{13}Sc_{57}(Rh_{13}Sc_{57})$			[10]
	$Ru_7Sc_{44}(Mg_{44}Rh_7)$		$Ru_7Sc_{44}(Mg_{44}Rh_7)$	-226
Zr	RuZr(B2)	RuZr(B2)	RuZr(B2)	-646
		$RuZr_4(D1_a)$		[7]
Hf	HfRu(B2)	N/A	HfRu(B2)	-819
	$HfRu_2$(unknown)			
Ti	RuTi(B2)	RuTi(B2)	RuTi(B2)	-763
		$RuTi_2$(C49)	$RuTi_2$(C49)	-532
		$RuTi_3(Mo_3Ti^*)$	$RuTi_3(Mo_3Ti^*)$	-401
Nb			$Nb_8Ru(Pt_8Ti)$	-117

Element	Compounds			ΔH
	Exper.	Calc.(Previous)	Calc.(Present)	meV/atom
		$Nb_5Ru(Nb_5Ru^*)$	$Nb_5Ru(Nb_5Ru^*)$	-172
		$Nb_3Ru(D0_3)$	$Nb_3Ru(L6_0)$	-222[9]
			$Nb_5Ru_3(Ga_3Pt_5)$	-249
	NbRu(unknown)			
			$Nb_3Ru_5(Ga_3Pt_5)$	-240
		$NbRu_2(C37)$		[11]
	$NbRu_3(L1_2)$	$NbRu_3(D0_{24})$		[8]
Ta	Ru_5Ta_3(unknown)	N/A	$Ru_5Ta_3(Ga_3Pt_5)$	-332
	RuTa(unknown)			
			$Ru_3Ta_5(Ga_3Pt_5)$	-313
			$RuTa_3(FCC^{[001]}_{AB3})$	-281
			$RuTa_5(Nb_5Ru^*)$	-207
V		N/A	$Ru_3V(Re_3Ru^*)$	-145
			$Ru_2V(C37)$	-192
	RuV(B11)			[28]
			$Ru_3V_5(Ga_3Pt_5)$	-313
			$RuV_2(C11_b)$	-321
			$RuV_3(Mo_3Ti^*)$	-296
			$RuV_4(D1_a)$	-262
			$RuV_5(Nb_5Ru^*)$	-230
			$RuV_8(Pt_8Ti)$	-154
Mo	σ	$MoRu_3(D0_{19})$	$MoRu_3(D0_{19})$	-56
W	σ	N/A	$Ru_3W(D0_{19})$	-65
Cr	σ	N/A	-	
Tc	-	$Ru_3Tc(D0_{19})$	$Ru_3Tc(D0_{19})$	-63
		RuTc(B19)	RuTc(B19)	-73
		$RuTc_3(D0_{19})$	$RuTc_3(D0_{19})$	-47
			$RuTc_5(RuTc_5^\star)$	-32
Mn	-	N/A	$Mn_{24}Ru_5(Re_{24}Ti_5)$	-15
Fe	-	N/A	-	
Os	-	N/A	$Os_3Ru(D0_a)$	-9
			OsRu(B19)	-15
			$OsRu_3(D0_a)$	-11
			$OsRu_5(Hf_5Sc^*)$	-9
Re	-	N/A	$Re_3Ru(Re_3Ru^*)$	-53
			ReRu(B19)	-86
			$ReRu_3(D0_{19})$	-80
Co	-	N/A	-	
Ir	-	N/A	$Ir_8Ru(Pt_8Ti)$	-20
			$Ir_3Re(L1_2)$	-34
			IrRu(B19)	-49
			$IrRu_2(C49)$	-54
			$IrRu_3(D0_{19})$	-53

Element	Compounds			ΔH
	Exper.	Calc.(Previous)	Calc.(Present)	meV/atom
			$IrRu_5(Hf_5Sc^*)$	-37
Rh	-		$Rh_8Ru(Pt_8Ti)$	-2
		$RhRu(RhRu^*)$	$RhRu(RhRu^*)$	-8
		$RhRu_2(RhRu_2^*)$	$RhRu_2(RhRu_2^*)$	-6
			$RhRu_5(RhRu_5^\star)$	-3
Ni	-	N/A	-	
Pt	-	$Pt_3Ru(FCC^{[001]}_{AB3})$		[4]
		$PtRu(FCC^{[001]}_{A2B2})$	PtRu(CdTi)	-33[1]
Pd	-	-	-	
Au	-	-	-	
Ag	-	-	-	
Cu	-	N/A	-	
Hg	-	N/A	-	
Cd	-	-	-	
Zn		N/A	$RuZn_3(L1_2)$	-150
	$RuZn_6(RuZn_6)$		$RuZn_6(RuZn_6)$	-132

Table 3.2: The newly found prototype which labeled as $\star$ in Table 3.1. Structures are fully relaxed by *ab initio* calculations.

Formula	$RhRu_5$	$RuTc_5$
Lattice	Orthorhombic	Monoclinic
Space Group (opt.)	Amm2 No.38	Cm #8 (2)
Pearson symbol	oS12	mS12
HT lattice type/variation	ORCC/ORCC	MCLC/MCLC1
Conv. Cell a, b, c (Å)	4.323, 2.724, 14.195	9.997, 2.752, 6.484
α, β, γ (deg)	90, 90, 90	90 75.942 90
Wyckoff positions	Rh1 0,0,0 (2a)	Ru1 0,0,-0.00140 (2a)
	Ru1 1/2,0,-0.223 (2b)	Tc1 0.390,0 -0.277 (2a)
	Ru2 0,0,-0.331 (2a)	Tc2 -0.335,0,-0.331 (2a)
	Ru3 1/2,0,0.444 (2b)	Tc3 0.055,0,0.388 (2a)
	Ru4 0,0 0.332 (2a)	Tc4 0.334,0,0.334 (2a)
	Ru5 1/2,0,0.112 (2b)	Tc5 -0.278,0,0.055 (2a)
AFLOW label	"141"	"128"

The NbRu system is attractive because of its shape-memory properties [Ghosh and Olson (2007); Shapiro et al. (2006); Tan et al. (2007); Benarchid et al. (2009); Mousa et al. (2009)]. This shape-memory alloy has two phases at high temperature. As temperature increases to 750°, the alloy forms a "β" phase that could be monoclinic or orthorhombic. Heating this alloy to 900° transforms it to an $L1_0$ structure, which is called "β." When the temperature exceeds 900°, the alloys transforms into a B2 structure that is also called the β phase. The interesting part is that one of these three compounds is found in our low-temperature calculations, but its stability is the same as found experimentally.

Fig. 3.4 shows that the convex hulls for OsRu, PtRu, and RhRu are lower than the others. The thermal contribution to free energy may be the principal factor that restricts the ordering at low temperature. Thus, we can obtain the vibrational contribution by calculating the phonon spectra. The OsRu energy was estimated by cluster expansion [Lerch et al. (2009)]. We find that the HT energy calculated is approximately 7 meV/atom lower than the energy estimated by cluster expansion. Furthermore, the transition temperature ($T_C \approx 110$K) is computed by Monte Carlo modeling with cluster expansion and the configuration entropy is the only element in cluster expansion. Thus, the vibrational contribution to energy is relatively small.

3.4 Technetium system

Current research on Tc alloy systems is based on two rationales. First, Tc is the only radioactive transition metal that forms alloys, and these alloys could be used for long-term nuclear-waste disposal [S. M. Frank and Marsden (2007)]. To achieve this goal, the fundamental properties of Tc-based alloys need to be better understood. Tc deposition on Au and TcZr binary alloys has been design for issue. Second, because Tc is a period 5 transition metal, investigating its alloy systems will provide a broad view of general material properties.

With *ab initio* calculations, we can predict properties that are difficult to obtain experimentally. In previous work, to investigate hcp, fcc, and bcc structures made from combining 76 elements, we used elastic constants and a zero-temperature equation [Shang et al. (2010)]. In addition, the stabilities of some complicated structures in the system were also calculated [Sluiter (2006)]. These results confirm that the ground state of Tc is an hcp structure. The hardness of Tc-based compounds has been investigated several times, in which analyses of Tc-based compounds led to the discovery of the superhardness of tungsten-related structures [Wang (2008, 2007); Wang et al. (2008)].

In addition to Ru systems, we also use the HT framework AFLOW to investigate Tc binary alloy systems. The results of AFLOW can be used to establish convex hulls for stability analysis. Our current research covers all Tc-transition-metal binary alloy systems and uses the generalized-gradient approximation and PAW pseudopotentials [Blöchl (1994)]. The free energies are calculated assuming zero temperature and pressure. In addition, spin polarization is included without lattice vibrations. The calculation structures are fully relaxed for lattice volume, lattice vectors, and atomic coordinates. The convergence tolerance is set to be 1 meV/atom, which is sufficient for crystal structure relaxation.

In this investigation, we calculated the possible crystal structures [Villars et al. (2004)] for every binary system. Up to 230 extra prototypes from the AFLOW prototype database [Curtarolo et al. (2012a)] are shown in [Levy et al. (2010b)]. From [Curtarolo et al. (2005)], we conclude that the probability of replicating experimentally determined stable structures is 96.7%. The theoretical calculations confirm the stable structures in not only compound-forming systems but also in noncompound-forming systems. Our calculations predict that the 9 of 14 noncompound-forming systems based on experiments [Villars et al. (2004)] have stable phases at zero temperature (see Fig. 3.7). In addition, we predicted extra stable compounds in four

compound-forming systems [Curtarolo et al. (2005)]: RhTc, RuTc, PtTc, and PdTc. The difference between the recent work and previous work reveals that our dataset has increased rapidly and that numerous uncovered compounds have been explored, including $Tc_{24}Ti_5$ and $Tc_{24}Zr_5$. We also discovered stable phases in a compound reported to be a disordered α phase.

Table 3.3: The data obtained from experiments ("Exper.") or from HT calculations ("Calc.") for Tc binary alloys and formation enthalpies ("ΔH"). $*$ represents the prototypes in previous work. $\star$ labels the one is newly discovered and showed in Table 3.4. "N/A" denotes no data. "-" indicates no compound.

Element	Compounds			ΔH
	Exper.	Calc.(Previous)	Calc.(Present)	meV/atom
Y	Tc_2Y(C14)	Tc_2Y(C14)	Tc_2Y(C14)	-176
		$TcY_3(D0_{11})$	$TcY_3(D0_{11})$	-86
Sc		N/A	$Sc_3Tc(D0_{11})$	-182
			$Sc_2Tc(C11_b)$	-208
	$ScTc_2$(C14)		$ScTc_2$(C14)	-304
	$Sc_{0.1}Tc_{0.9}(\chi)$		$Sc_5Tc_{24}(Re_{24}Ti_5)$	-189
Zr	$Tc_{0.88}Zr_{0.12}(\chi)$		$Tc_{24}Zr_5(Re_{24}Ti_5)$	-186
	Tc_2Zr(C14)	Tc_2Zr(C14)	Tc_2Zr(C14)	-314
	TcZr(unknown)	TcZr(B2)	TcZr(B2)	-356
		$TcZr_2$(C49)	$TcZr_2$(C49)	-271
		$TcZr_4(D1_a)$	$TcZr_4(D1_a)$	-186
Hf		N/A	$Hf_3Tc(Mo_3Ti^*)$	-269
			Hf_2Tc(C49)	-357
	HfTc(B2)		HfTc(B2)	-482
	$HfTc_2$(C14)		$HfTc_2$(C14)	-362
	$Hf_{0.1}Tc_{0.9}(\chi)$		$Hf_5Tc_{24}(Re_{24}Ti_5)$	-232
Ti	$Tc_{0.9}Ti_{0.1}(\chi)$		$Tc_{24}Ti_5(Re_{24}Ti_5)$	-190
		$Tc_2Ti(C11_b)$		[18]
			$Tc_5Ti_3(Ga_3Pt_5)$	-416
	TcTi(B2)	TcTi(B2)	TcTi(B2)	-492
		$TcTi_2$(C49)	$TcTi_2$(C49)	-376
		$TcTi_3(Mo_3Ti^*)$	$TcTi_3(Mo_3Ti^*)$	-298
Nb			$Nb_5Tc(HfPd_5^*)$	-144
		$Nb_3Tc(Mo_3Ti^*)$	$Nb_3Tc(Mo_3Ti^*)$	-213
		$Nb_2Tc(C11_b)$	$Nb_2Tc(C11_b)$	-279
		NbTc(B2)	NbTc(B2)	-365
	$Nb_{0.15}Tc_{0.85}(\chi)$			[19]
Ta		N/A	$Ta_2Tc(C11_b)$	-388

Element	Compounds			ΔH
	Exper.	Calc.(Previous)	Calc.(Present)	meV/atom
	TaTc(B2)		TaTc(B2)	-501
	$Ta_{0.15}Tc_{0.85}(\chi)$			[36]
V	TcV(B2)	N/A	TcV(B2)	-377
			$TcV_2(C11_b)$	-340
			$TcV_3(Mo_3Ti^*)$	-266
			$TcV_4(D1_a)$	-218
Mo	$Mo_{1.5}Tc_{2.4}$(A15)	N/A	-	
	$Mo_{0.3}Tc_{0.7}(\sigma)$			
W	$Tc_{0.7}W_{0.3}(\sigma)$	N/A	-	
Cr	$Cr_{0.25}Tc_{0.75}(\sigma)$	N/A	-	
Re	-	N/A	$ReTc_3(D0_{11})$	-5
Mn	$Mn_{0.4}Tc_{0.6}(\sigma)$	N/A	Mn_2Tc(C14)	-94
Fe	FeTc(B2)	N/A		[158]
	$Fe_{0.4}Tc_{0.6}(\sigma)$		$FeTc_2$(C16)	-4
Os	-	N/A	$Os_3Tc(D0_{19})$	-71
			OsTc(B19)	-83
			$OsTc_3(D0_{19})$	-57
Ru	-	$Ru_3Tc(D0_{19})$	$Ru_3Tc(D0_{19})$	-63
		RuTc(B19)	RuTc(B19)	-73
		$RuTc_3(D0_{19})$	$RuTc_3(D0_{19})$	-47
			$RuTc_5(RuTc_5^\star)$	-32
Co	-	N/A	CoTc(B19)	-46
			$CoTc_3(D0_{19})$	-53
Ir	-	N/A	$Ir_8Tc(Pt_8Ti)$	-89
			$Ir_2Tc(Ir_2Tc^\star)$	-224
			IrTc(B19)	-287
			$IrTc_3(D0_{19})$	-217
Rh	-	$Rh_2Tc(ZrSi_2)$	$Rh_2Tc(Ir_2Tc^\S)$	-157
		RhTc(B19)	RhTc(B19)	-175
		$RhTc_3(D0_{19})$	$RhTc_3(D0_{19})$	-158
Ni	-	N/A	$Ni_4Tc(D1_a)$	-30
			$NiTc_3(D0_{19})$	-106
Pt	-	$Pt_3Tc(FCC_{AB3}^{[001]})$	$Pt_3Tc(BCC_{AB3}^{[001]})$	-158
			$Pt_2Tc(CuZr_2)$	-184
		$PtTc_3(D0_{19})$	$PtTc_3(D0_{19})$	-267
Pd	-		PdTc(RhRu*)	-63
		$PdTc_3(D0_{19})$	$PdTc_3(D0_{19})$	-73
Au	-	-	-	
Ag	-	-	-	
Cu	-	-	-	
Hg	-	-	-	
Cd	-	-	-	
Zn		N/A	$Tc_2Zn(FCC_{AB2}^{[100]})$	-42

Element	Compounds			ΔH
	Exper.	Calc.(Previous)	Calc.(Present)	meV/atom
			$TcZn_3(L1_2)$	-62
	$TcZn_7(CuPt_7)$		$TcZn_7(CuPt_7)$	-55
	$TcZn_{15}$(unknown)			

The results of the calculation are shown in Table 3.3. The first column presents the 28 metals that form alloy systems with Ru, ordered by Mendeleev numbers [Pettifor (1986)]. The following three columns contain the data that determine whether the system can form stable compounds given experimental data, current HT calculations, and previous HT calcualtions [Curtarolo et al. (2005)].

Table 3.4: The newly found prototype which labeled as $\star$ in Table 3.1. Structures are fully relaxed by *ab initio* calculations.

Formula	Ir_2Tc	$RuTc_5$
Lattice	Orthorhombic	Monoclinic
Space Group (opt.)	Cmcm No.63	Cm No.8 (2)
Pearson symbol	oS12	mS12
HT lattice type/variation	ORCC/ORCC	MCLC/MCLC1
Conv. Cell a, b, c (Å)	2.751,14.374,4.381	9.997, 2.752, 6.484
α, β, γ (deg)	90, 90, 90	90 75.942 90
Wyckoff positions	Ir1 0,0.998,1/4 (4c) Ir2 0,0.668,1/4 (4c) Tc1 0,0.334,1/4 (4c)	Ru1 0,0,-0.00140 (2a) Tc1 0.390,0 -0.277 (2a) Tc2 -0.335,0,-0.331 (2a) Tc3 0.055,0,0.388 (2a) Tc4 0.334,0,0.334 (2a) Tc5 -0.278,0,0.055 (2a)
AFLOW label	"143"	"128"

The Mendeleev number is the most efficient single parameter by which whether alloy systems have stable phases can be predicted [Villars et al. (2001)]. With this

parameter, we can easily classify the binary systems into several clusters. This classification provides a predictive insight for binary alloy systems [Pettifor (1986)]. As mentioned above, Tc is a radioactive element, and hence the predictive power is restricted by the experimental data [Villars et al. (2001)]. From this perspective, *ab initio* calculations are important for the design and discovery of Tc-related systems. In Table 3.3, we provide three clusters for experimental data. From the top to TcV in the table, all the systems listed could have stable structures, except NbTc, which is expected to be a disordered χ phase. The bottom cluster, from OsTc to the end, contains the noncompound-forming systems. Similar to Ru, Zn-based alloy systems also form stable compounds but with a low Medeleev constant. Most systems between these two clusters are the disordered α phase; ReTc, which is phase separating, and FeTc, which has a stable structure in order to be a disordered α phase. We consider the results of our calculations to be distinct from the experimental results. Three systems, FeTc, MnTc, and ReTc, are predicted to form compounds in the bottom cluster. From OsTc to PdTc, these eight systems also form ordered phases. Thus, overall, the table gives eleven systems that form stable compounds. The compounds $X\mathrm{Tc}_3$ (X = Os or Ru) with prototype $\mathrm{D0}_{19}$ appears to have ordered phases. Three structures in this section, containing $\mathrm{Ir}_2\mathrm{Tc}$, $\mathrm{Rh}_2\mathrm{Tc}$, and RuTc_5, are predicted by the HT methods but have no known *Strukturbericht* designation or prototypes. These structures were designed from the superlattice structure in the AFLOW prototype database [Curtarolo et al. (2005)]. These newly found structures are listed in Table 3.4.

The system NbTc has also been predicted to form compounds. The top cluster has eight continuous ordered phase systems. At the bottom of Table 3.3, TcZn remains the only compound-forming system listed. In this binary system, our results indicate that two unknown compounds are stable: $\mathrm{Tc}_2\mathrm{Zn}$ and TcZn_3. Furthermore, we discover no structure similar to TcZn_{15}, which was found experimentally.

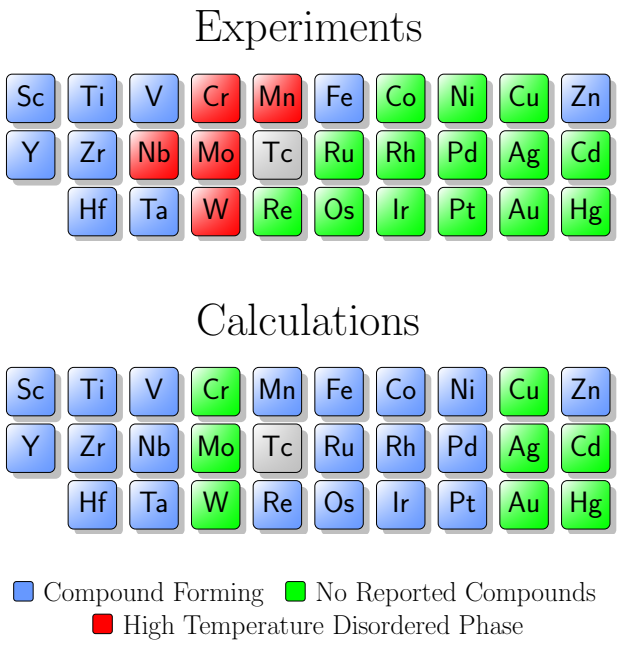

FIGURE 3.7: Technetium binary systems in the periodic table: phase separating (green), high-temperature disordered (red), and miscible (blue).

3.5 Ternary phase diagrams

In the previous chapter, we showed that binary systems utilize 2D convex hulls for stability study. Currently, we are planning to implement high-dimensional convex hulls for multicomponent systems. But only 3D and 4D systems are considered for the visualization problem.

Similar to binary systems, we have to construct a coordinate system which contains component information for each element and the formation energy of each compound. Then the convex hulls in 3D and 4D space will be determined by AFLOW. With this convex hull, visualization should be considered. Thus we have to project 3D to 2D and 4D to 3D to form a triangle and a tetrahedron respectively. For these two polyhedrons, each corner represents an element. The lines connecting them and the space between them will be the unique compounds for the systems.

We designed algorithm for 3D convex hulls and applied this efficient alogrithm in confirming the stability of 9 ternary systems, which is an on going study. These systems include Al-Co-Mn, Al-Fe-Mn, Al-Mn-Ni, Co-Fe-P, Co-Mn-Ga, Co-Mn-Ge, Co-Mn-P, Fe-Ga-Mn, and Fe-Ge-Mn. In figures 3.8 - 3.12 are projection of 3D convex hulls for 5 selected systems. In these pictures, black "+" represents the stable compounds inside the phasediagrams; red "×" indicates that structure should be the closest compound to surface of convex hull. Under each compound name, if it is a stable compound, there is an "E_F", which is the formation enthalpy of that compound, if not, there is an extra parameter labeled "Dis" which reveals the distance from that compound to surface of convex hull a measure of the "instability" of that compound.

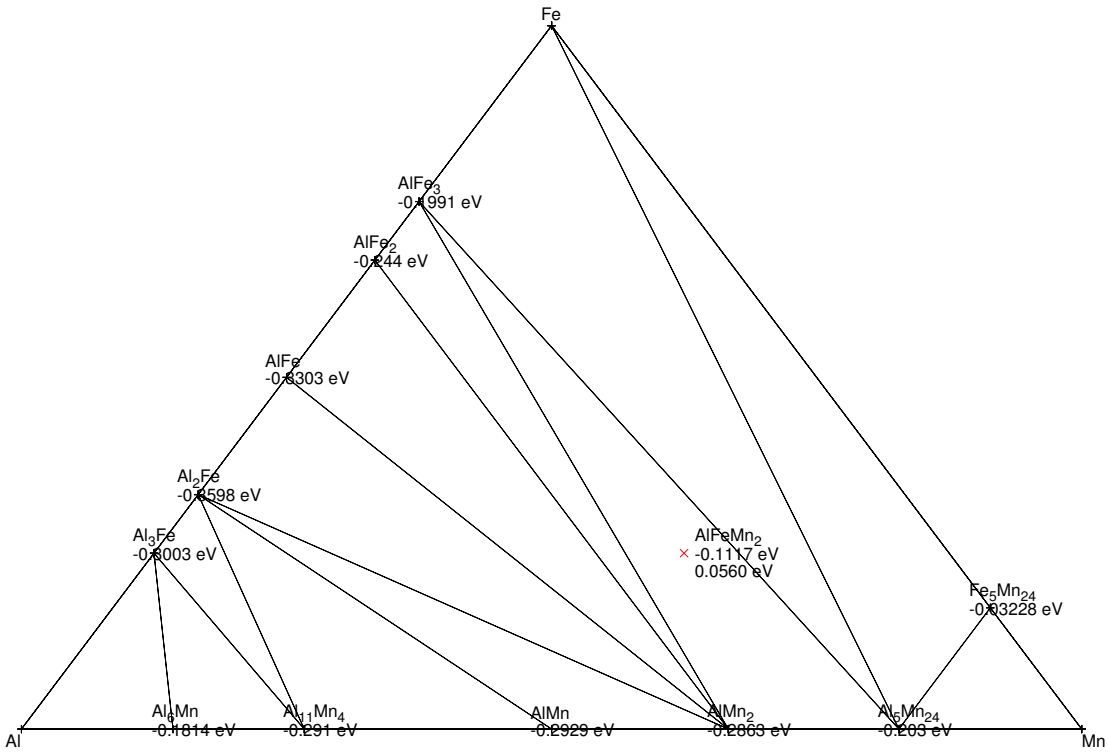

FIGURE 3.8: Ternary convex hull projection of Al-Fe-Mn systems.

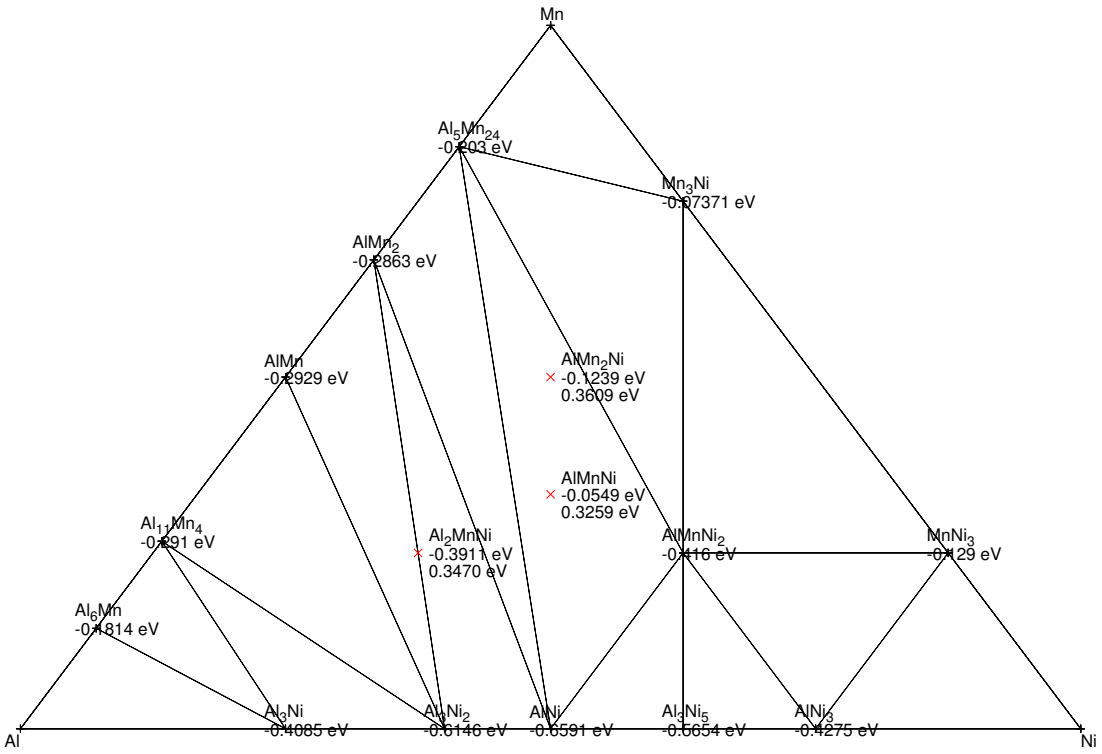

FIGURE 3.9: Ternary convex hull projection of Al-Mn-Ni systems.

3.6 Conclusions

In summary, computational investigation of material phase diagrams is an efficient method for discovering new materials. Studying the energies of newly designed structures at low temperature is a good method to check stability, which is an important material property. For Ru systems, the binary alloys from our study are distinct from experimental results and from other previous work because of the large dataset that we have exploited. We discovered stable phases in two disordered α systems and in seven noncompound-forming systems, which are recorded as experimental data. Furthermore, we considered not only the thermodynamic equilibrium at zero temperature but also the vibrational and configurational contributions, which may weaken the stability of predicted structures. Because Tc is radioactive, the experimental data are incomplete for this element, but Tc-related compounds can still be

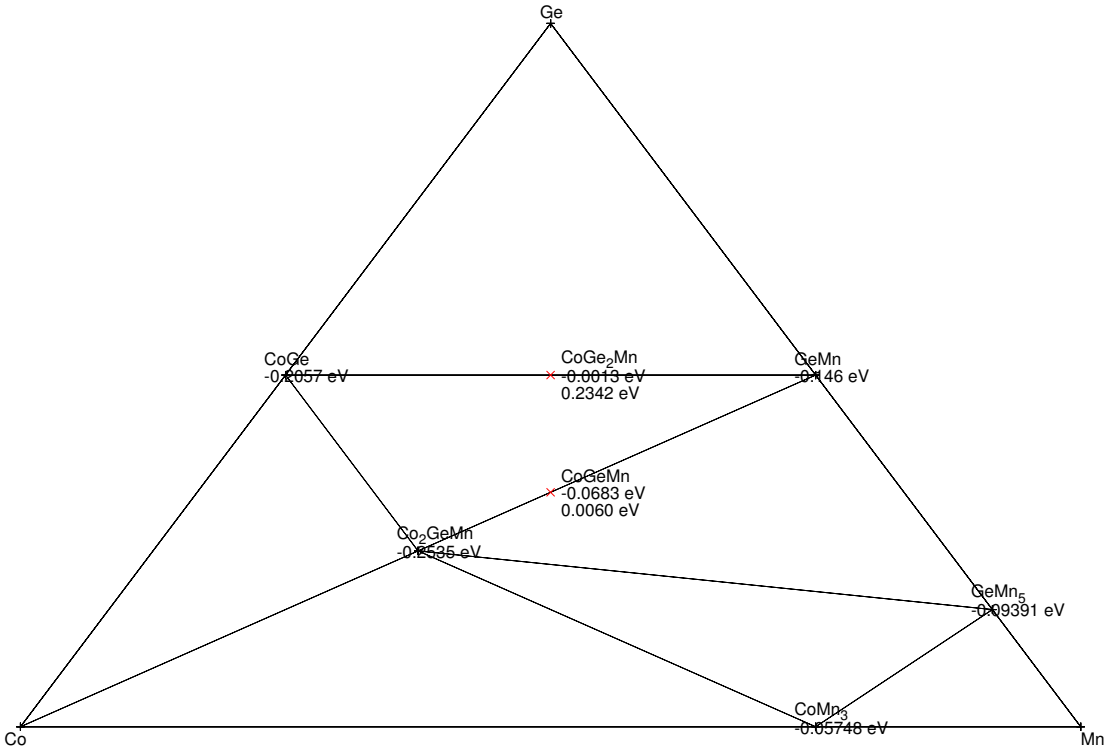

FIGURE 3.10: Ternary convex hull projection of Co-Ge-Mn systems.

investigated by our method. These computational results could be a guide for future material design and discovery.

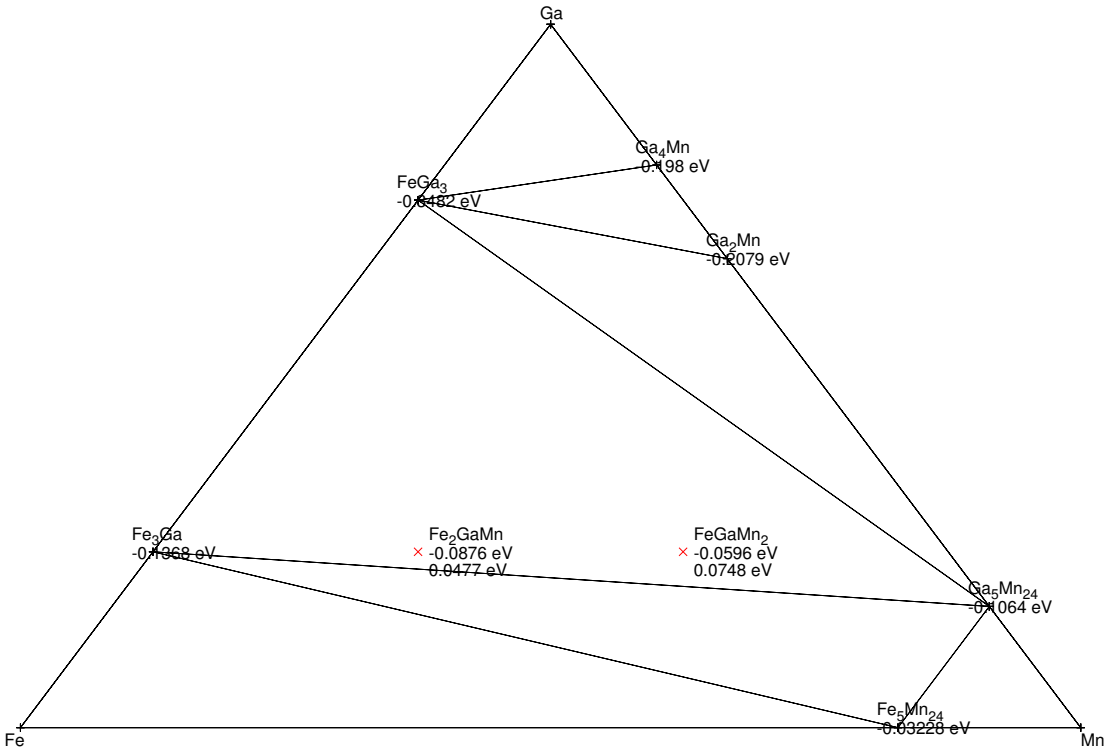

FIGURE 3.11: Ternary convex hull projection of Fe-Ga-Mn systems.

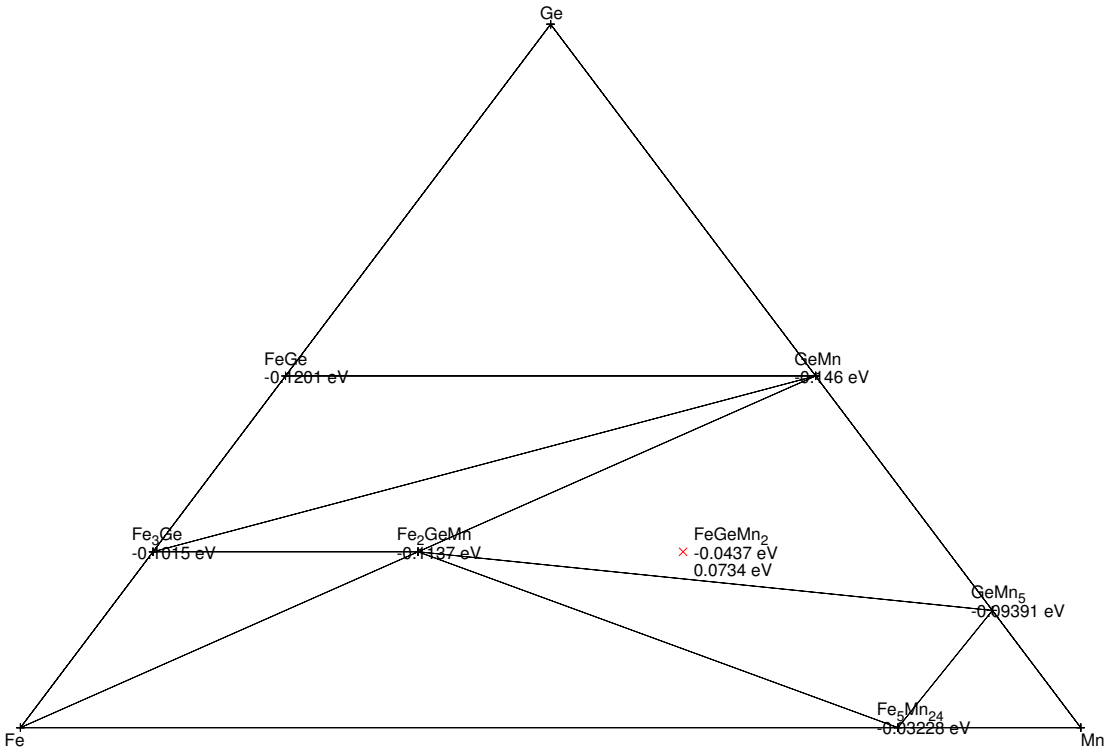

FIGURE 3.12: Ternary convex hull projection of Fe-Ge-Mn systems.

Bibliography

Bagchi, J. and Bhattacharya, S. (2008), "Studies of the electrocatalytic activity of binary palladium ruthenium anode catalyst on Ni support for ethanol alkaline fuel cells," *Transition Metal Chemistry*, 33, 113–120.

Baker, H., Bennett, L. H., Massalski, T. B., and Murray, J. L. (1986), *Binary alloy phase diagrams*, American Society of Metals, Metals Park, OH.

Belsky, A., Hellenbrandt, M., Karen, V. L., and Luksch, P. (2002), "New developments in the Inorganic Crystal Structure Database (ICSD): accessibility in support of materials research and design," *Acta Cryst.*, B58, 364–369.

Benarchid, M., David, N., Fiorani, J.-M., Vilasi, M., and Benlaharche, T. (2009), "Enthalpies of formation of NbRu and NbRuAl alloys," *Thermochimica Acta*, 482, 39 – 41.

Bever, M. (1985), *Encyclopedia of materials science and engineering*.

Bleskov, I. D., Smirnova, E. A., Vekilov, Y. K., Korzhavyi, P. A., Johansson, B., Katsnelson, M., Vitos, L., Abrikosov, I. A., and Isaev, E. I. (2009), "Ab initio calculations of elastic properties of Ru[sub 1 - x]Ni[sub x]Al superalloys," *Applied Physics Letters*, 94, 161901.

Blöchl, P. E. (1994), "Projector augmented-wave method," *Phys. Rev. B*, 50, 17953–17979.

Boyer, L. L., Stokes, H. T., and Mehl, M. J. (1995), "Self-Consistent potential induced breathing model calculations for longitudinal modes in MgO," *Ferroelectrics*, 164, 177–181.

Brown, I. D., Abrahams, S. C., Berndt, M., Faber, J., Karen, V. L., Motherwell, W. D. S., Villars, P., Westbrook, J. D., and McMahon, B. (2005), "Report of the Working Group on Crystal Phase Identifiers," *Acta Cryst.*, A61, 575–580.

Brunner, G. O. (1971), "An unconventional view of the 'closest sphere packings'," *Acta Crystallographica Section A*, 27, 388–390.

Chen, H., Zhu, W., and Zhang, Z. (2010), "Contrasting Behavior of Carbon Nucleation in the Initial Stages of Graphene Epitaxial Growth on Stepped Metal Surfaces," *Phys. Rev. Lett.*, 104, 186101.

Curtarolo, S., Morgan, D., Persson, K., Rodgers, J., and Ceder, G. (2003), "Predicting Crystal Structures with Data Mining of Quantum Calculations," *Phys. Rev. Lett.*, 91, 135503.

Curtarolo, S., Morgan, D., and Ceder, G. (2005), "Accuracy of ab initio methods in predicting the crystal structures of metals: A review of 80 binary alloys," *Calphad*, 29, 163 – 211.

Curtarolo, S., Setyawan, W., Hart, G. L., Jahnatek, M., Chepulskii, R. V., Taylor, R. H., Wang, S., Xue, J., Yang, K., Levy, O., Mehl, M. J., Stokes, H. T., Demchenko, D. O., and Morgan, D. (2012a), "AFLOW: An automatic framework for high-throughput materials discovery," *Computational Materials Science*, 58, 218 – 226.

Curtarolo, S., Setyawan, W., Hart, G. L., Jahnatek, M., Chepulskii, R. V., Taylor, R. H., Wang, S., Xue, J., Yang, K., Levy, O., Mehl, M. J., Stokes, H. T., Demchenko, D. O., and Morgan, D. (2012b), "AFLOW: An automatic framework for high-throughput materials discovery," *Computational Materials Science*, 58, 218 – 226.

Daams, J. L. C., van Vucht, J. H. N., and Villars, P. (1992), "Atomic-environment classification of the cubic intermetallic structure types," *J. Alloys Compound.*, 182, 1–33.

Desai, S. K. and Neurock, M. (2003), "First-principles study of the role of solvent in the dissociation of water over a Pt-Ru alloy," *Phys. Rev. B*, 68, 075420.

en Jiang, D., Du, M.-H., and Dai, S. (2009), "First principles study of the graphene/Ru(0001) interface," *The Journal of Chemical Physics*, 130, 074705.

Eschrig, M., Kopu, J., Cuevas, J. C., and Schön, G. (2003), "Theory of Half-Metal/Superconductor Heterostructures," *Phys. Rev. Lett.*, 90, 137003.

Fogden, A. (1993), "Parametrization of triply periodic minimal surfaces. III. General algorithm and specific examples for the irregular class," *Acta Crystallographica Section A*, 49, 409–421.

Gajdoš, M., Hummer, K., Kresse, G., Furthmüller, J., and Bechstedt, F. (2006), "Linear optical properties in the projector-augmented wave methodology," *Phys. Rev. B*, 73, 045112.

Ghosh, G. and Olson, G. (2007), "Integrated design of Nb-based superalloys: Ab initio calculations, computational thermodynamics and kinetics, and experimental results," *Acta Materialia*, 55, 3281 – 3303.

Gong, X.-F., Yang, G. X., Fu, Y. H., Xie, Y. Q., Zhuang, J., and Ning, X.-J. (2009), "First-principles study of Ni/Ni3Al interface strengthening by alloying elements," *Computational Materials Science*, 47, 320 – 325.

Grns, O., Korzhavyi, P., Kissavos, A., and Abrikosov, I. (2008), "Theoretical study of the MoRu sigma phase," *Calphad*, 32, 171 – 176.

Gus L. W. Hart, Volker Blum, M. J. W. and Zunger, A. (2005), "Evolutionary approach for determining first-principles hamiltonians," *Nat Mater*, 4, 391 – 394.

Hart, G. L. W. and Forcade, R. W. (2008), "Algorithm for generating derivative structures," *Phys. Rev. B*, 77, 224115.

Hart, G. L. W. and Forcade, R. W. (2009), "Generating derivative structures from multilattices: Algorithm and application to hcp alloys," *Phys. Rev. B*, 80, 014120.

Hasan, M. Z. and Kane, C. L. (2010), "*Colloquium* : Topological insulators," *Rev. Mod. Phys.*, 82, 3045–3067.

He, X., Kong, L., Li, J., Li, X., and Liu, B. (2006), "Structure stability and magnetic properties of the NiRu system studied by ab initio and molecular dynamics calculations together with ion beam mixing," *Acta Materialia*, 54, 3375 – 3381.

He, X., Liang, S.-H., Li, J.-H., and Liu, B.-X. (2007), "Atomistic mechanism of interfacial reaction and asymmetric growth kinetics in an immiscible Cu-Ru system at equilibrium," *Phys. Rev. B*, 75, 045431.

He, X., Wang, W.-C., and Liu, B.-X. (2008), "Ferromagnetic states in Fe-Ru systems studied by *ab initio* calculation and ion-beam mixing," *Phys. Rev. B*, 77, 012401.

Žutić, I., Fabian, J., and Das Sarma, S. (2004), "Spintronics: Fundamentals and applications," *Rev. Mod. Phys.*, 76, 323–410.

Jahnátek, M., Levy, O., Hart, G. L. W., Nelson, L. J., Chepulskii, R. V., Xue, J., and Curtarolo, S. (2011), "Ordered phases in ruthenium binary alloys from high-throughput first-principles calculations," *Phys. Rev. B*, 84, 214110.

Jóhannesson, G. H., Bligaard, T., Ruban, A. V., Skriver, H. L., Jacobsen, K. W., and Nørskov, J. K. (2002), "Combined Electronic Structure and Evolutionary Search Approach to Materials Design," *Phys. Rev. Lett.*, 88, 255506.

Karen, V. L. and Hellenbrandt, M. (2002), "Inorganic crystal structure database: new developments," *Acta Cryst.*, A58, c367.

Kissavos, A., Shallcross, S., Meded, V., Kaufman, L., and Abrikosov, I. (2005), "A critical test of ab initio and {CALPHAD} methods: The structural energy difference between bcc and hcp molybdenum," *Calphad*, 29, 17 – 23.

Kissavos, A. E., Shallcross, S., Kaufman, L., Grånäs, O., Ruban, A. V., and Abrikosov, I. A. (2007), "Thermodynamics of ordered and disordered phases in the binary Mo-Ru system," *Phys. Rev. B*, 75, 184203.

Kolmogorov, A. N., Calandra, M., and Curtarolo, S. (2008), "Thermodynamic stabilities of ternary metal borides: An *ab initio* guide for synthesizing layered superconductors," *Phys. Rev. B*, 78, 094520.

Kong, Y., Li, J. H., Kong, L. T., and Liu, B. X. (2005), "Role of spatial valence charge density on the metastability of an immiscible binary metal system at equilibrium," *Phys. Rev. B*, 72, 024209.

Kresse, G. and Hafner, J. (1993), "*Ab initio* molecular dynamics for liquid metals," *Phys. Rev. B*, 47, 558–561.

Lerch, D., Wieckhorst, O., Hart, G. L. W., Forcade, R. W., and Mller, S. (2009), "UNCLE: a code for constructing cluster expansions for arbitrary lattices with minimal user-input," *Modelling and Simulation in Materials Science and Engineering*, 17, 055003.

Levy, O., Hart, G. L., and Curtarolo, S. (2010a), "Hafnium binary alloys from experiments and first principles," *Acta Materialia*, 58, 2887 – 2897.

Levy, O., Hart, G. L. W., and Curtarolo, S. (2010b), "Structure maps for hcp metals from first-principles calculations," *Phys. Rev. B*, 81, 174106.

Levy, O., Jahntek, M., Chepulskii, R. V., Hart, G. L. W., and Curtarolo, S. (2011), "Ordered Structures in Rhenium Binary Alloys from First-Principles Calculations," *Journal of the American Chemical Society*, 133, 158–163.

Lewis, G., Sachtler, J., Low, J., Lesch, D., Faheem, S., Dosek, P., Knight, L., Halloran, L., Jensen, C., Yang, J., Sudik, A., Siegel, D. J., Wolverton, C., Ozolins, V., and Zhang, S. (2007), "High throughput screening of the ternary LiNH2MgH2LiBH4 phase diagram," *Journal of Alloys and Compounds*, 446447, 355 – 359, Proceedings of the International Symposium on Metal-Hydrogen Systems, Fundamentals and Applications (MH2006).

Maradudin, A. A., Montroll, E. W., Weiss, G. H., and P., I. I. (1971), *Theory of lattice dynamics in the harmonic approximation*, Academic Press, New York.

Mehl, M. (2012), "Naval Research Laboratory Crystal Structure Database," `http://cst-www.nrl.navy.mil/lattice/`.

Mighell, A. D. and Karen, V. L. (1993), "NIST materials science databases," *Acta Cryst.*, A49, c409.

Monkhorst, H. J. and Pack, J. D. (1976), "Special points for Brillouin-zone integrations," *Phys. Rev. B*, 13, 5188–5192.

Mousa, A. A., Hamad, B. A., and Khalifeh, J. M. (2009), "Structure, electronic and elastic properties of the NbRu shape memory alloys," *The European Physical Journal B*, 72, 575–581.

Nakatsuji, N. (1978), "Cluster expansion of the wavefunction. Excited states," *Chemical Physics Letters*, 59, 362 – 364.

Okamoto, Y. (2004), "Finding optimum compositions of catalysts using ab initio calculations and data mining," *Chemical Physics Letters*, 395, 279 – 284.

Ortiz, C., Eriksson, O., and Klintenberg, M. (2009), "Data mining and accelerated electronic structure theory as a tool in the search for new functional materials," *Computational Materials Science*, 44, 1042 – 1049.

Ozolins, V., Majzoub, E. H., and Wolverton, C. (2008), "First-Principles Prediction of a Ground State Crystal Structure of Magnesium Borohydride," *Phys. Rev. Lett.*, 100, 135501.

P. Villars, L. C. (1991), *Pearsons Handbook of Crystallographic Data for Intermetallic Phases*, ASM International, Materials Park, OH.

Peng, X. and Ahuja, R. (2010), "Epitaxial graphene monolayer and bilayers on Ru(0001): *Ab initio* calculations," *Phys. Rev. B*, 82, 045425.

Pettifor, D. (1984), "A chemical scale for crystal-structure maps," *Solid State Communications*, 51, 31 – 34.

Pettifor, D. G. (1986), "The structures of binary compounds. I. Phenomenological structure maps," *Journal of Physics C: Solid State Physics*, 19, 285.

Pickett, W. E. and Moodera, J. S. (2001), "Half Metallic Magnets," *Physics Today*, 54, 39–44.

Prez, G., Pastor, E., and Zinola, C. (2009), "A novel Pt/Cr/Ru/C cathode catalyst for direct methanol fuel cells (DMFC) with simultaneous methanol tolerance and oxygen promotion," *International Journal of Hydrogen Energy*, 34, 9523 – 9530.

S. M. Frank, D. D. K. and Marsden, K. C. (2007), *Immobilization of Technetium in a Metallic Waste Form*, American Nuclear Society, La Grange Park, Illinois.

Sanchez, J., Ducastelle, F., and Gratias, D. (1984), "Generalized cluster description of multicomponent systems," *Physica A: Statistical Mechanics and its Applications*, 128, 334 – 350.

Setyawan, W. and Curtarolo, S. (2010), "High-throughput electronic band structure calculations: Challenges and tools," *Computational Materials Science*, 49, 299 – 312.

Setyawan, W., Gaume, R. M., Lam, S., Feigelson, R. S., and Curtarolo, S. (2011), "High-Throughput Combinatorial Database of Electronic Band Structures for Inorganic Scintillator Materials," *ACS Combinatorial Science*, 13, 382–390.

Shang, S., Saengdeejing, A., Mei, Z., Kim, D., Zhang, H., Ganeshan, S., Wang, Y., and Liu, Z. (2010), "First-principles calculations of pure elements: Equations of state and elastic stiffness constants," *Computational Materials Science*, 48, 813 – 826.

Shapiro, S. M., Xu, G., Gu, G., Gardner, J., and Fonda, R. W. (2006), "Lattice dynamics of the high-temperature shape-memory alloy Nb-Ru," *Phys. Rev. B*, 73, 214114.

Shin, D., Arróyave, R., Liu, Z.-K., and Van de Walle, A. (2006), "Thermodynamic properties of binary hcp solution phases from special quasirandom structures," *Phys. Rev. B*, 74, 024204.

Sluiter, M. (2006), "Ab initio lattice stabilities of some elemental complex structures," *Calphad*, 30, 357 – 366.

Snyder, G. J. and Toberer, E. S. (2008), "Complex thermoelectric materials," *Nat Mater*, 7, 105–114.

Spišák, D., Lorenz, R., and Hafner, J. (2001), "Structure and magnetism in thin films and multilayers of hexagonal ruthenium and iron," *Phys. Rev. B*, 63, 094424.

Stucke, D. P. and Crespi, V. H. (2003), "Predictions of New Crystalline States for Assemblies of Nanoparticles: Perovskite Analogues and 3-D Arrays of Self-Assembled Nanowires," *Nano Letters*, 3, 1183–1186.

Tan, C., Cai, W., and Tian, X. (2007), "Structural, electronic and elastic properties of NbRu high-temperature shape memory alloys," *Scripta Materialia*, 56, 625 – 628.

Taniguchi, A., Akita, T., Yasuda, K., and Miyazaki, Y. (2004), "Analysis of electrocatalyst degradation in PEMFC caused by cell reversal during fuel starvation," *Journal of Power Sources*, 130, 42 – 49.

Taylor, R. H., Curtarolo, S., and Hart, G. L. W. (2011), "Guiding the experimental discovery of magnesium alloys," *Phys. Rev. B*, 84, 084101.

Villars, P. and Daams, J. (1993), "Atomic-environment classification of the chemical elements," *Journal of Alloys and Compounds*, 197, 177 – 196, Proceeding of the Workshop on Regularities, Classifications and Prediction of Advanced Materials.

Villars, P., Brandenburg, K., Berndt, M., LeClair, S., Jackson, A., Pao, Y.-H., Igelnik, B., Oxley, M., Bakshi, B., Chen, P., and Iwata, S. (2001), "Binary, ternary and quaternary compound former/nonformer prediction via Mendeleev number," *Journal of Alloys and Compounds*, 317318, 26 – 38, The 13th International Conference on Solid Compounds of Transition Elements.

Villars, P., Berndt, M., Brandenburg, K., Cenzual, K., Daams, J., Hulliger, F., Massalski, T., Okamoto, H., Osaki, K., Prince, A., Putz, H., and Iwata, S. (2004), "The Pauling File, Binaries Edition," *Journal of Alloys and Compounds*, 367, 293 – 297, Proceedings of the VIII International Conference on Crystal Chemistry of Intermetallic Compounds.

Wang, B., Gnther, S., Wintterlin, J., and Bocquet, M.-L. (2010a), "Periodicity, work function and reactivity of graphene on Ru(0001) from first principles," *New Journal of Physics*, 12, 043041.

Wang, M., Li, Y., Cui, T., Ma, Y., and Zou, G. (2008), "Origin of hardness in WB[sub 4] and its implications for ReB[sub 4], TaB[sub 4], MoB[sub 4], TcB[sub 4], and OsB[sub 4]," *Applied Physics Letters*, 93, 101905.

Wang, S., Wang, Z., Setyawan, W., Mingo, N., and Curtarolo, S. (2011), "Assessing the Thermoelectric Properties of Sintered Compounds via High-Throughput *Ab-Initio* Calculations," *Phys. Rev. X*, 1, 021012.

Wang, W. C., Shen, Y. X., Li, J. H., Li, X. Y., and Liu, B. X. (2006), "Formation and structural transformation of the nonequilibrium phases in the RuTa system induced by ion beam mixing," *Journal of Physics: Condensed Matter*, 18, 9911.

Wang, W. C., Dai, Y., Wang, T. L., Li, J. H., He, X., and Liu, B. X. (2009), "Magnetic properties of some metastable Co–Ru alloys studied by ion beam mixing and ab initio calculation," *Applied Physics Letters*, 94, 131903.

Wang, Y.-J. and Wang, C.-Y. (2008), "A first-principles survey of the partitioning behaviors of alloying elements on gamma/gamma[sup [prime]] interface," *Journal of Applied Physics*, 104, 013109.

Wang, Y. X. (2007), "Elastic and electronic properties of TcB[sub 2] and superhard ReB[sub 2]: First-principles calculations," *Applied Physics Letters*, 91, 101904.

Wang, Y. X. (2008), "Ultra-incompressible and hard technetium carbide and rhenium carbide: First-principles prediction," *physica status solidi (RRL) Rapid Research Letters*, 2, 126–128.

Wang, Z.-B., Zhao, C.-R., Shi, P.-F., Yang, Y.-S., Yu, Z.-B., Wang, W.-K., and Yin, G.-P. (2010b), "Effect of a Carbon Support Containing Large Mesopores on the Performance of a PtRuNi/C Catalyst for Direct Methanol Fuel Cells," *The Journal of Physical Chemistry C*, 114, 672–677.

White, P. S., Rodgers, J. R., and Le Page, Y. (2002), "CRYSTMET: a database of the structures and powder patterns of metals and intermetallics," *Acta Crystallographica Section B*, 58, 343–348.

Wolverton, C., Siegel, D. J., Akbarzadeh, A. R., and Ozoli, V. (2008), "Discovery of novel hydrogen storage materials: an atomic scale computational approach," *Journal of Physics: Condensed Matter*, 20, 064228.

Yu, X.-X. and Wang, C.-Y. (2009), "The effect of alloying elements on the dislocation climbing velocity in Ni: A first-principles study," *Acta Materialia*, 57, 5914 – 5920.

Biography

Junkai Xue was born November 11, 1986 in Zhenjiang, Jiangsu, China. He attended Zhenjiang No.1 High School in China and completed his Bachelors degree in Nanjing University of Technology from 2005 to 2009.

After 2009, he received his Master of Science in July of 2012. His doctoral research, guided by Dr. Stefano Curtarolo, focused on high-throughput computational materials science.